Article

SOURCE DATA | TRANSPARENT PROCESS | OPEN ACCESS

EMBO reports

The obesity-linked human lncRNA AATBC stimulates mitochondrial function in adipocytes

Maude Giroud[1,2,3,4,†], Stefan Kotschi[4,†], Yun Kwon[1,2,3], Ophélia Le Thuc[5], Anne Hoffmann[6], Manuel Gil-Lozano[1,2,3], Michael Karbiener[7], Juan Carlos Higareda-Almaraz[1,2,3], Sajjad Khani[1,4], Daniel Tews[8], Pamela Fischer-Posovszky[8], Wenfei Sun[9], Hua Dong[9], Adhideb Ghosh[9], Christian Wolfrum[9], Martin Wabitsch[8], Kirsi A Virtanen[10], Matthias Blüher[6,11], Søren Nielsen[12], Anja Zeigerer[1,2,3], Cristina García-Cáceres[2,5,13], Marcel Scheideler[1,2,3], Stephan Herzig[1,2,3,14,*] & Alexander Bartelt[1,4,15,16,**]

Abstract

Adipocytes are critical regulators of metabolism and energy balance. While white adipocyte dysfunction is a hallmark of obesity-associated disorders, thermogenic adipocytes are linked to cardiometabolic health. As adipocytes dynamically adapt to environmental cues by functionally switching between white and thermogenic phenotypes, a molecular understanding of this plasticity could help improving metabolism. Here, we show that the lncRNA Apoptosis associated transcript in bladder cancer (AATBC) is a human-specific regulator of adipocyte plasticity. Comparing transcriptional profiles of human adipose tissues and cultured adipocytes we discovered that AATBC was enriched in thermogenic conditions. Using primary and immortalized human adipocytes we found that AATBC enhanced the thermogenic phenotype, which was linked to increased respiration and a more fragmented mitochondrial network. Expression of AATBC in adipose tissue of mice led to lower plasma leptin levels. Interestingly, this association was also present in human subjects, as AATBC in adipose tissue was inversely correlated with plasma leptin levels, BMI, and other measures of metabolic health. In conclusion, AATBC is a novel obesity-linked regulator of adipocyte plasticity and mitochondrial function in humans.

Keywords adipocyte; mitochondrial dynamics; non-coding RNA; obesity; thermogenesis
Subject Categories Metabolism; RNA Biology
DOI 10.15252/embr.202357600 | Received 5 June 2023 | Revised 31 July 2023 | Accepted 10 August 2023 | Published online 6 September 2023
EMBO Reports (2023) 24: e57600

Introduction

Adipocytes are critical regulators of energy metabolism and nutrient homeostasis, and their dysfunction is tightly linked to metabolic disorders. While in humans, metabolic disease is mainly associated with white adipocytes, thermogenic adipocytes in brown adipose tissue (BAT) are associated with metabolic health (van Marken Lichtenbelt *et al*, 2009; Chondronikola *et al*, 2014; Leitner *et al*, 2017; U Din *et al*, 2018). These cells are diverse in nature and display high phenotypic plasticity (Bartelt & Heeren, 2014). Their primary

1 Institute for Diabetes and Cancer, Helmholtz Center Munich, Neuherberg, Germany
2 German Center for Diabetes Research, Neuherberg, Germany
3 Joint Heidelberg-IDC Translational Diabetes Program, Inner Medicine 1, Heidelberg University Hospital, Heidelberg, Germany
4 Institute for Cardiovascular Prevention, Faculty of Medicine, Ludwig-Maximilians-University, Munich, Germany
5 Institute for Diabetes and Obesity, Helmholtz Center Munich, Neuherberg, Germany
6 Helmholtz Institute for Metabolic, Obesity and Vascular Research of the Helmholtz Zentrum München at the University of Leipzig and University Hospital Leipzig, Leipzig, Germany
7 Global Pathogen Safety, Baxter AG, Vienna, Austria
8 Division of Pediatric Endocrinology and Diabetes, Department of Pediatrics and Adolescent Medicine, Ulm University Medical Center, Ulm, Germany
9 Institute of Food, Nutrition and Health, ETH Zürich, Schwerzenbach, Switzerland
10 Turku PET Centre, Turku University Hospital, Turku, Finland
11 Medical Department III – Endocrinology, Nephrology, Rheumatology, University of Leipzig Medical Center, Leipzig, Germany
12 The Centre of Inflammation and Metabolism and the Centre for Physical Activity Research, Rigshospitalet, University of Copenhagen, Copenhagen, Denmark
13 Medizinische Klinik and Poliklinik IV, Klinikum der Universität, Ludwig-Maximilians-Universität München, Munich, Germany
14 Chair Molecular Metabolic Control, Technical University Munich, Munich, Germany
15 German Center for Cardiovascular Research, Partner Site Munich Heart Alliance, Ludwig-Maximilians-University, Munich, Germany
16 Department of Molecular Metabolism & Sabri Ülker Center, Harvard T.H. Chan School of Public Health, Boston, MA, USA
*Corresponding author. Tel: +49 89 3187 1045; E-mail: stephan.herzig@helmholtz-muenchen.de
**Corresponding author. Tel: +49 89 4400 43905; E-mail: alexander.bartelt@med.uni-muenchen.de
†These authors contributed equally to this work

function is non-shivering thermogenesis (NST), mediated by Uncoupling protein 1 (UCP1) and UCP1-independent futile cycling mechanisms (de Meis, 2001; Ukropec *et al*, 2006; Anunciado-Koza *et al*, 2008; Keipert *et al*, 2017; Tajima *et al*, 2020). When humans are subjected to cold, thermogenic adipocytes increase their metabolic activity, and if the exposure is sustained, thermogenic adipocytes are also recruited in white adipose tissue (WAT), an adaptive phenomenon referred to as adipose tissue browning (van Marken Lichtenbelt *et al*, 2009; Virtanen *et al*, 2009), or, conversely, adipose tissue whitening (Shimizu & Walsh, 2015). In mice, thermoneutrality is ca. 30°C (Cannon & Nedergaard, 2011), but humans are thermoneutral at much lower temperatures and, therefore, humans only display limited thermogenic activity (de Jong *et al*, 2019). However, in colder regions, people display marked NST (van Marken Lichtenbelt *et al*, 2009), indicating that the environmental temperature are major determinant of BAT activity. Furthermore, activating BAT has remarkable benefits for metabolic health in mouse models of metabolic disorders (Bartelt *et al*, 2011, 2017; Berbee *et al*, 2015), but also, in the general population, BAT is linked to better cardiometabolic health (Becher *et al*, 2021). Understanding the molecular switches regulating thermogenic plasticity in adipocytes might help to develop novel therapies for treating obesity-associated metabolic disorders (Giroud *et al*, 2022).

Key aspects of thermogenic plasticity include facilitating an increase of mitochondrial respiration in response to cold, and conversely, directing the involution of mitochondrial capacity when the adipocytes return to a non-thermogenic state at thermoneutrality. In most cells, a fragmented mitochondrial network is associated with stress, whereas fused mitochondria are thought to display enhanced respiration (Giacomello *et al*, 2020). In the case of adipocytes, mitochondrial dynamics are largely regulated by nutrient availability and depend on the thermogenic status of the adipocyte (Quiros *et al*, 2012; Pisani *et al*, 2018; Dai & Jiang, 2019; Ruan *et al*, 2020). The interplay of molecules governing these mitochondrial adaptations are complex and involve a large panel of transcriptional and posttranslational regulators, for example peroxisome proliferator-activated receptor co-activator 1-alpha (PGC1α) (Puigserver *et al*, 1998), Nuclear factor erythroid-2, like-1 (NFE2L1, also known as NRF1 or TCF11; Bartelt *et al*, 2018), Mitofusin-1 and -2 (MFN1 and MFN2; Wikstrom *et al*, 2014;Boutant *et al*, 2017; Mahdaviani *et al*, 2017), OPA1 mitochondrial dynamin like GTPase (OPA1; Rogne *et al*, 2018; Pereira *et al*, 2021) as well as dynamin 1 like (DNM1L, also known as DRP1; Pisani *et al*, 2018). For example, adipocyte-specific Mfn2-deficient mice display blunted mitochondrial fusion and impaired adaptative thermogenesis (Boutant *et al*, 2017; Mahdaviani *et al*, 2017). In human adipocytes, it has been shown previously that an acute activation of thermogenic adipocytes involves fission of the mitochondrial network for enhanced respiration (Wikstrom *et al*, 2014; Pisani *et al*, 2018).

In addition to these transcriptional and posttranslational mechanisms, non-coding RNAs and especially long non-coding RNAs (lncRNAs) have emerged as potential regulators of adipocyte function (Lo *et al*, 2018; Schmidt *et al*, 2018; Dallner *et al*, 2019; Sun & Lin, 2019; Zhang *et al*, 2021). The number of lncRNAs in the genome is correlated with organism complexity, they are highly tissue-specific, and their sequence is only poorly conserved between species (Eisenberg & Levanon, 2013). Typically, lncRNAs are longer than 200 nucleotides and bind to many types of molecules including RNA, DNA, amino acids, and proteins (Kazimierczyk *et al*, 2020). In addition to their interactome, their cellular localization also defines their function. For example, when localized to the nucleus, lncRNA impact transcriptional control, genomic imprinting, and chromatin condensation (MacDonald & Mann, 2020). Furthermore, in the cytoplasm, lncRNAs are decoys for mRNA translation and miRNA function, thus affecting mRNA turnover (Statello *et al*, 2021). The study of lncRNAs in metabolism is an emerging field. In adipocytes, lncRNA have been linked to adipogenesis (Zhang *et al*, 2021). For example, Brown fat lncRNA 1 (Blnc1) and brown adipose tissue–enriched lncRNA 10 (lncBATE10) promote the development of thermogenic adipocytes through the regulation of Early B Cell Factor 2 (EBF2) and PGC1α, respectively (Alvarez-Dominguez *et al*, 2015; Zhao *et al*, 2015; Bai *et al*, 2017). CCCTC-binding factor (zinc finger protein)-like, opposite strand (Ctcflos) was described as a regulator of browning via regulation of PR/SET Domain 16 (PRDM16) splicing (Bast-Habersbrunner *et al*, 2021). However, most of these lncRNAs are specific to mice and are not found in humans. One study found 318 lncRNAs conserved in humans and mice (Ding *et al*, 2018). To the best of our knowledge, LINC00473 is so far the only non-conserved, human lncRNA implicated in the regulation of thermogenic adipocytes (Tran *et al*, 2020).

In the current study, we set out to discover new lncRNAs specific to human adipocytes and linked to NST and obesity. Based on a transcriptional comparative analysis between human WAT and BAT as well as adrenergic stimulation of different models of cultured human adipocytes, we show that the lncRNA Apoptosis associated transcript in bladder cancer (AATBC) (Zhao *et al*, 2015; Tang *et al*, 2020; Wang *et al*, 2021; Yan *et al*, 2021), regulates thermogenic plasticity of adipocytes by stimulating mitochondrial dynamics and respiration, and is linked to human obesity.

Results

Identification of AATBC as a human lncRNA linked to NST *in vivo* and *in vitro*

Investigating the phenotypic signatures of different adipose depots in humans as well as isolated adipocytes offers the opportunity to unravel novel lncRNAs implicated in the control of thermogenic plasticity. Therefore, we performed a combined RNAseq analysis of three different human models. We compared lncRNA expression profiles of (i) WAT and BAT *ex vivo*, (ii) differentiated human primary adipose-derived stem (hpAS) cells treated with norepinephrine (NE) and (iii) human adipose derived stem (hMADS) cells treated with forskolin (Fig 1A). To confirm the induction of the thermogenic phenotype, we quantified *UCP1* mRNA expression in all samples (Fig 1C–E). Other thermogenic markers such as citrate synthase (*CS*), cell death inducing DFFA like effector A (*CIDEA*), peroxisome proliferator-activated receptor gamma coactivator 1-α (*PPARGC1A*) and adipose markers such as peroxisome proliferator-activated receptor-γ (*PPARG*), perilipin 1 (*PLIN1*) and fatty acid binding protein 4 (*FABP4*) were quantified for quality control purposes (Appendix Fig S1G–X). After rigorous filtering (Appendix Fig S1A–D), we found 368 lncRNAs to be differentially regulated in WAT vs BAT, 105 lncRNAs in hpAS treated with NE compared to control cells, and 116 lncRNAs in hMADS stimulated with forskolin compared to

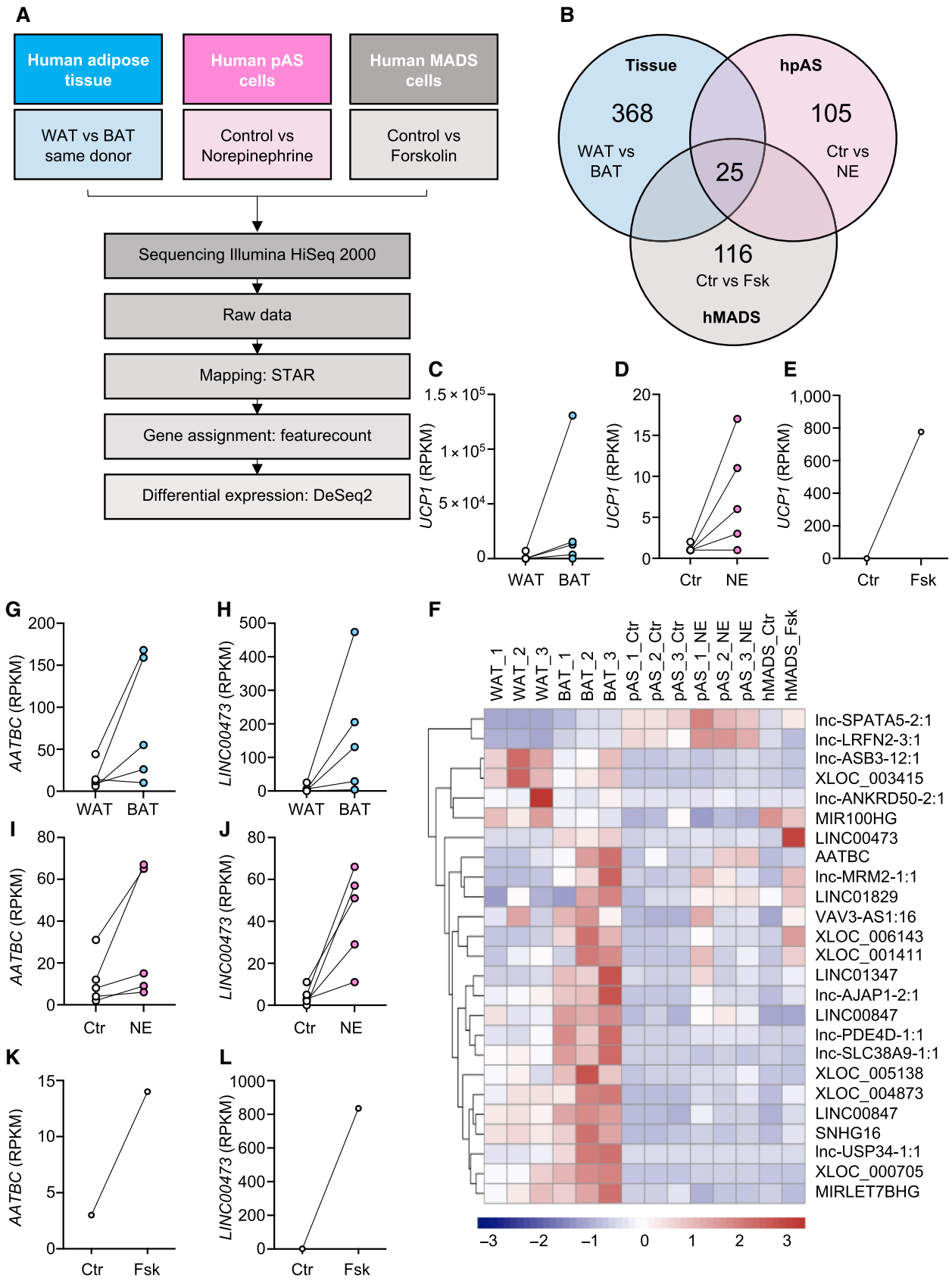

Figure 1.

Figure 1. Identification of the lncRNA AATBC linked to thermogenesis in humans.

A Experimental outline.
B Venn diagram of regulated lncRNA.
C–E *UCP1* expression in (C) human brown and white adipose tissue, (D) human primary adipocytes treated with 1 μM norepinephrine for 6 h and (E) hMADS cells treated at day 15 of differentiation with 1 μM forskolin for 6 h (C: $n = 5$ patients, D: $n = 5$ replicates, E: $n = 1$ replicate).
F Heatmap of the differential expression of lncRNAs ($n = 1$–3 replicates).
G–L Expression of *AATBC* and *LINC00473* (G, H: $n = 5$ subjects; I, J: $n = 5$ replicates; K, L: $n = 1$ replicate).

control cells, respectively. Out of these differentially regulated set of lncRNAs, 25 candidates were regulated in the same fashion under all three conditions (Fig 1B). Among these, we found that the majority of lncRNAs had higher expression levels under thermogenic conditions (Fig 1F and Appendix Fig S1E and F). Interestingly, among the lncRNAs with unknown function in adipocytes, the lncRNA AATBC was one of the most prominent candidates, which was consistently upregulated in all three models of stimulated thermogenesis. Of note, we found that LNC00473 was consistently upregulated, which is in agreement with a previous study on human lncRNAs (Tran *et al*, 2020). These findings indicate that our stratification strategy was valid. (Fig 1F–L and Appendix Fig S1E and F). In summary, the thermogenic phenotype of adipocytes is characterized by an induction of lncRNA transcription. In the pool of upregulated lncRNAs, AATBC is consistently associated with increased thermogenesis in human adipose tissue and cultured adipocyte models.

AATBC is a nuclear lncRNA induced by thermogenic activation and differentiation

As AATBC matched the candidate profile for a lncRNA associated with thermogenic features, we further explored the nature and regulation of AATBC expression in our *in vitro* models of human adipocytes. Confirming the results of the initial RNASeq screening, AATBC expression was higher in primary human brown adipocytes treated with NE (Fig 2A and B). As adipocyte browning is also induced by chronic PPARγ activation (Petrovic *et al*, 2010), we treated hSVF with the PPARγ agonist rosiglitazone during the differentiation (Appendix Fig S2A–C). Also, in this distinct model of adipocyte browning AATBC expression was higher under thermogenic conditions compared to controls cells differentiated to classical white adipocytes (Fig 2C). Using adipose tissue fractionation, we found that AATBC was expressed at higher levels in differentiated adipocytes compared to SVF cells (Fig 2D). Also, in hMADS cells we observed higher levels of AATBC in the respective models of thermogenic and regular differentiation (Fig 2E and F). *UCP1*, *PLIN1*, *and FABP4* expression levels as well as lipid content served as validation markers for the thermogenic and regular differentiation, respectively (Appendix Fig S2D–N). Next to expression levels, the localization of lncRNAs is very important for understanding their function. To this end, we separated nuclear and cytoplasmic RNA from differentiated thermogenic hMADS cells (Fig 2J and K) and found that AATBC was enriched in the nuclear fraction (Fig 2I). The finding that AATBC is a nuclear lncRNA was corroborated by in situ hybridization of AATBC (RNAscope®) in the same hMADS cells. There, endogenous expression of AATBC was detected in the nucleus. (Fig 2L). This observation was confirmed by overexpression of AATBC, after which in most cells AATBC was found in the nucleus (Fig 2M). In summary, our data demonstrate that AATBC is a nuclear lncRNA and is induced by thermogenic activation and differentiation.

Modulation of AATBC expression regulates mitochondrial oxygen consumption

To investigate the biological significance of AATBC we performed loss and gain-of-function experiments in human adipocytes. We used anti-sense oligonucleotide (ASO)-mediated knockdown of AATBC in hMADS cells under thermogenic conditions, where otherwise AATBC expression is high, and adenoviral over-expression of AATBC in regular hMADS cells, where otherwise AATBC expression is low (Fig 3A). Using two independent ASOs we found that AATBC silencing led to lower *UCP1* expression (Fig 3B and C). These observations were confirmed in primary cells derived from hSVF (Appendix Fig S3A and B). Similarly, an alternative approach using siRNA

Figure 2. AATBC is associated with adipocyte browning and found in the nucleus.

A, B *AATBC* expression in (A) white or (B) brown human stromal-vascular fraction (hSVF) cells treated with 1 μM norepinephrine for 6 h ($n = 5$ technical replicates from 3 biological experiments).
C *AATBC* expression in hSVF differentiated to a white and thermogenic phenotype ($n = 7$ technical replicates from three biological experiments).
D *AATBC* expression in the SVF, adipocyte fraction (AF) and total fraction (TF) of human white adipose tissue ($n = 9$ technical replicates from three biological experiments).
E, F *AATBC* expression in (E) white or (F) thermogenic human mesenchymal adipose stem (hMADS) cells treated with 1 μM norepinephrine for 6 h ($n = 9$ technical replicates from three biological experiments).
G *AATBC* expression in hMADS cells differentiated to a white and thermogenic phenotype ($n = 9$ technical replicates from three biological experiments).
H *AATBC* expression in undifferentiated and differentiated hMADS cells ($n = 12$ technical replicates from three biological experiments).
I–K Expression of *AATBC*, *12S* and *U1* mRNA in the nucleus and cytosol of thermogenic hMADS cells ($n = 8$ technical replicates from three biological experiments).
L, M *In situ* hybridization (RNAScope®) of *AATBC* in thermogenic hMADS cells at (L) untreated conditions and (M) in thermogenic hMADS treated with adenovirus (AV)-mediated overexpression (OE) of *AATBC* (or control AV) (representative images from three independent experiments) (M). Scale bars: 20 μm and 5 μm for the magnified images.

Data information: Statistical significance *$P < 0.05$ by 2-tailed, unpaired Student's *T*-test (A, C–K) or 2-way ANOVA followed by Tukey's test (B) Data are presented ± s.e.m.
Source data are available online for this figure.

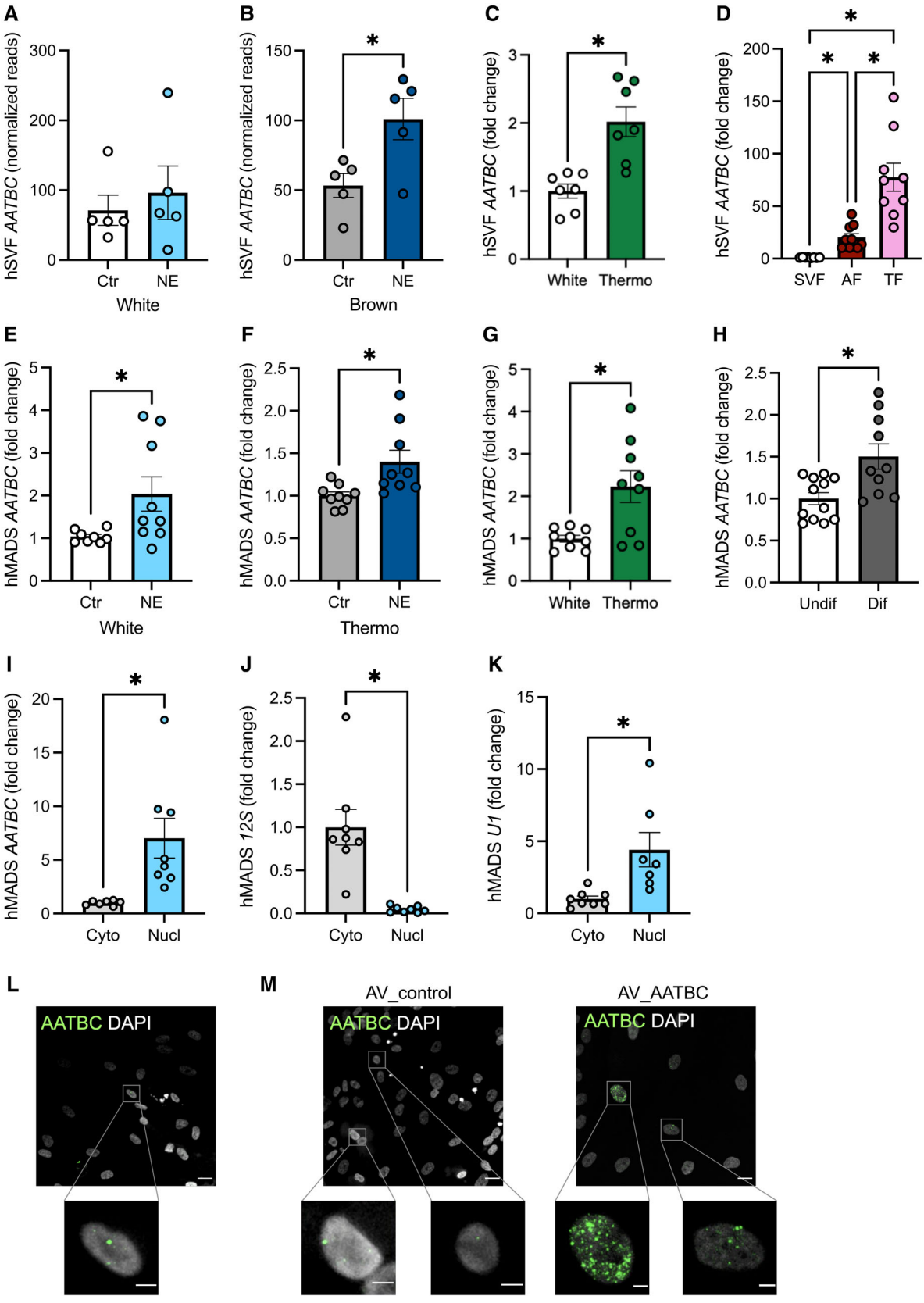

Figure 2.

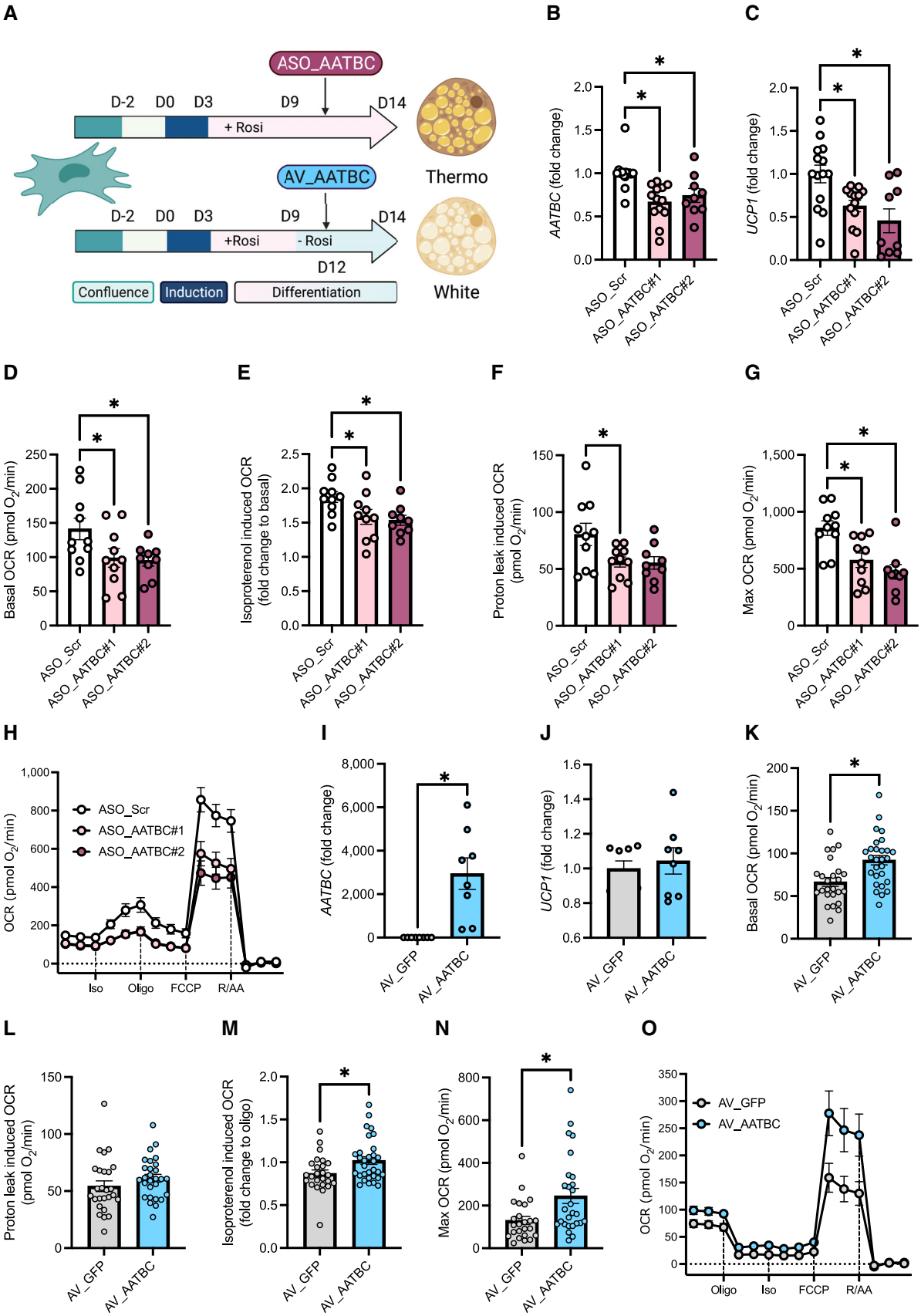

Figure 3.

Figure 3. AATBC is a regulator of mitochondrial function.

A Experimental outline.

B, C Expression of *AATBC* and *UCP1* during anti-sense oligonucleotide (ASO)-mediated knockdown of *AATBC* (n = 9–15 technical replicates from five biological experiments).

D–H Oxygen consumption rate (OCR) during ASO-mediated knockdown of *AATBC* visualized as (H) trace or cumulative at (D) baseline measurement, (E) isoproterenol-induced OCR, (F) oligomycin (Oligo) induced proton leak or (G) carbonyl cyanide-4-(trifluoromethoxy)phenylhydrazone (FCCP)-induced maximal respiration (D–G: n = 10 technical replicates from a representative experiment, H: representative trace).

I, J Expression of *AATBC* and *UCP1* during adenovirus (AV)-mediated overexpression of *AATBC* (n = 8 technical replicates from three biological experiments).

K–O OCR during ASO-mediated knockdown of *AATBC* visualized as (O) trace or cumulative at (K) baseline measurement, (L) isoproterenol-induced OCR, (M) OCR after oligomycin (Oligo) or (N) FCCP-induced maximal respiration (K–N: n = 27 technical replicates, O: representative trace).

Data information: Statistical significance *P < 0.05 by 2-way ANOVA followed by Tukey's test (B–G) or 2-tailed unpaired Student's T-test (I–N). Data are presented ± s.e.m.

against AATBC led to similar results in hMADS cells (Appendix Fig S3E and F). As changes in UCP1 levels might indicate altered mitochondrial function, we assessed the bioenergetic profiles of hMADS with silenced AATBC and control cells. We found that silencing of AABTC diminished basal, isoproterenol-stimulated, uncoupled respiration as well as lower spare mitochondrial capacity (Fig 3D–H). Taken together, this data set indicates that loss of AATBC disrupts the thermogenic function of adipocytes. In the complementary approach, we found that after overexpression of AATBC *UCP1* expression remained unchanged (Fig 3I and J). Yet we observed higher basal respiration and higher spare mitochondrial capacity compared to control cells. However, isoproterenol-stimulated respiration and proton leak remained unchanged, which is in line with the unchanged UCP1 expression (Fig 3K–O). Of note, *PLIN1* and *FABP4* expression levels were largely unchanged, indicating that manipulation of AATBC did not interfere with adipogenesis per se (Appendix Fig S3C, D and G–L). Next, we investigated if the manipulation of AATBC function is linked to any transcriptional changes that could explain the mitochondrial phenotype. We silenced AATBC in thermogenic hMADS using siRNA and performed RNASeq. We found that despite a marked reduction in AATBC levels, the effect on global gene regulation was minor and only few genes were impacted by the loss of AATBC without any clear outcome (Appendix Fig S4A–C). We also performed a transcriptomic analysis of regular hMADS overexpressing AATBC and found lipid and triglyceride metabolism pathways to be regulated (Appendix Fig S4D–F). Regardless of these observations, the transcriptomic changes upon of AATBC manipulation were not immediately linked to mitochondrial function, potentially indicating the AATBC exerts its effects largely via posttranscriptional mechanisms.

Modulation of AATBC expression regulates mitochondrial dynamics

Considering that AATBC had only minor impact on the transcriptome of thermogenic adipocytes, we hypothesized that the mitochondrial phenotype is manifested at the posttranslational level. First, we quantified mitochondria DNA, but neither inhibition nor overexpression of AATBC led to altered mitochondrial DNA levels, suggesting that the number of mitochondria was unchanged under these conditions (Appendix Fig S5A and B). Next, we investigated mitochondrial dynamics, as mitochondrial fission and fusion events regulate mitochondrial respiration (Quiros *et al*, 2012; Thaher *et al*, 2018). Using TOM20 immunostaining, we found that silencing of AATBC in thermogenic hMADS was associated with higher numbers and length of mitochondrial branches as well as more mitochondrial junctions per cell area compared to control cells (Fig 4A–D). These observations illustrate a link between AATBC, mitochondrial network connectivity, and increased thermogenic function. As mitochondrial fusion is mediated in part by OPA1 and MFN2, we evaluated their protein levels. We found that compared to control cells the levels of both proteins were higher in hMADS cells upon knockdown of AATBC (Fig 4E–G), indicating a shift in mitochondrial dynamics towards fusion. We also measured protein levels of the different OXPHOS complexes, which remained unchanged (Fig 4H). Complementary to this data set, overexpression of AATBC was associated with less mitochondrial connectivity (Fig 4I–L) and lower OPA1 but unchanged MFN2 and OXPHOS levels compared to control-infected cells (Fig 4M–P). In summary, these data demonstrate that modulation of AATBC expression regulates mitochondrial dynamics.

Figure 4. AATBC modulates mitochondrial dynamics by promoting fission.

A TOMM20 staining and image analysis of white hMADS cells (representative image of three independent experiments, scale bar: 10 μm).

B–D Quantification of (B) length of mitochondrial branches, (C) junctions per cell area, and (D) branches per cell area (n = 24 cells observed).

E–G Immunoblot of OPA1, MFN2, and β-tubulin and the respective quantification normalized to β-Tubulin levels (E: representative immunoblot; F, G: n = 15 technical replicates replicates from five biological experiments).

H Immunoblot of OXPHOS complexes.

I TOMM20 staining and image analysis of white hMADS cells (representative image of three independent experiments, scale bar: 10 μm).

J–L Quantification of (K) length of mitochondrial branches, (L) junctions per cell area and (M) branches per cell area (n = 24 cells observed).

M–O Immunoblot of OPA1, MFN2, and β-Tubulin and the respective quantification normalized to β-Tubulin levels (M: representative immunoblot; N: n = 15 technical replicates from five biological experiments; O: n = 6 technical replicates from three biological experiments).

P Immunoblot of OXPHOS complexes.

Data information: Statistical significance *P < 0.05 by 2-tailed unpaired Student's T-test (B–D, F, G, J–L, N, O). Data are presented ± s.e.m.

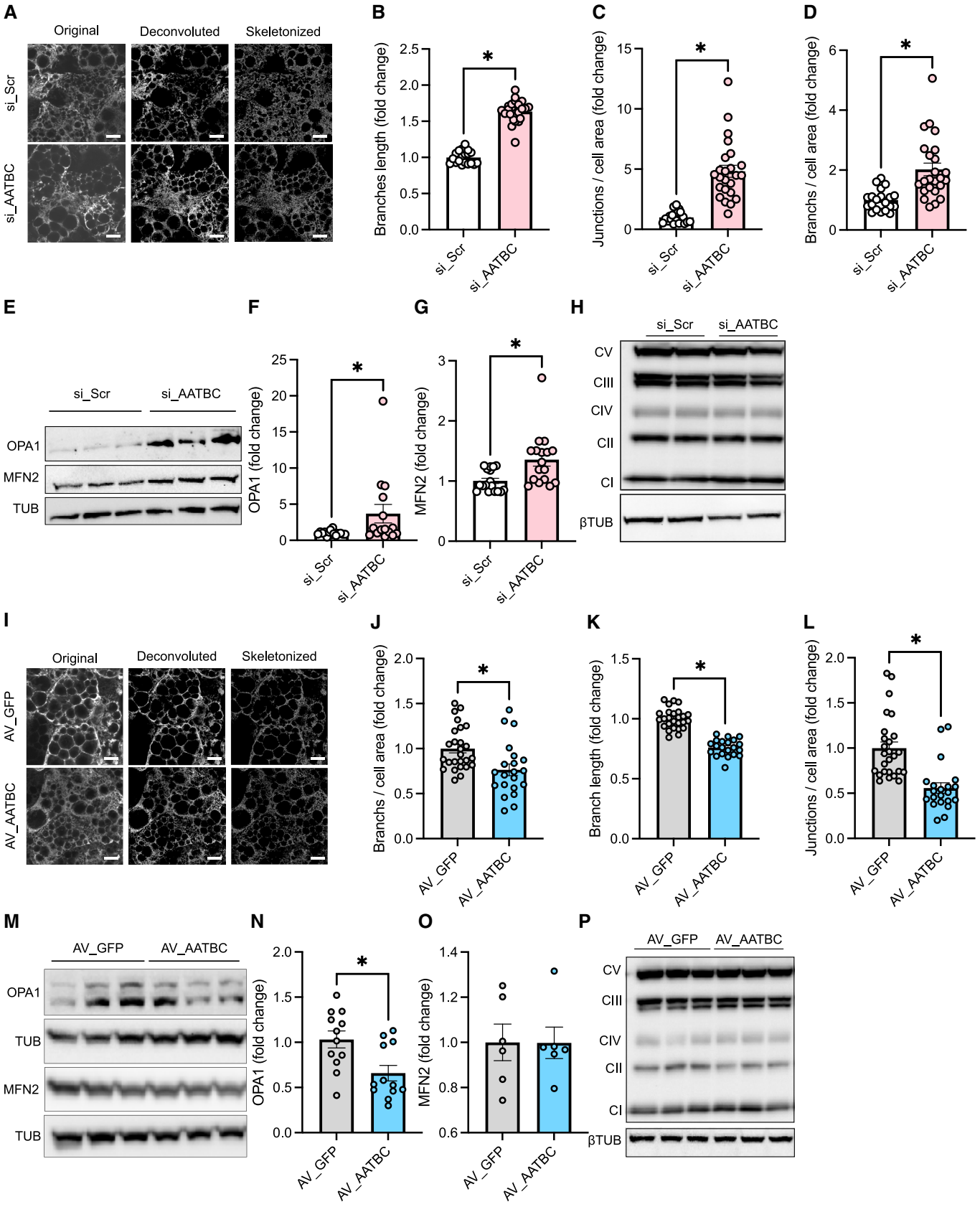

Figure 4.

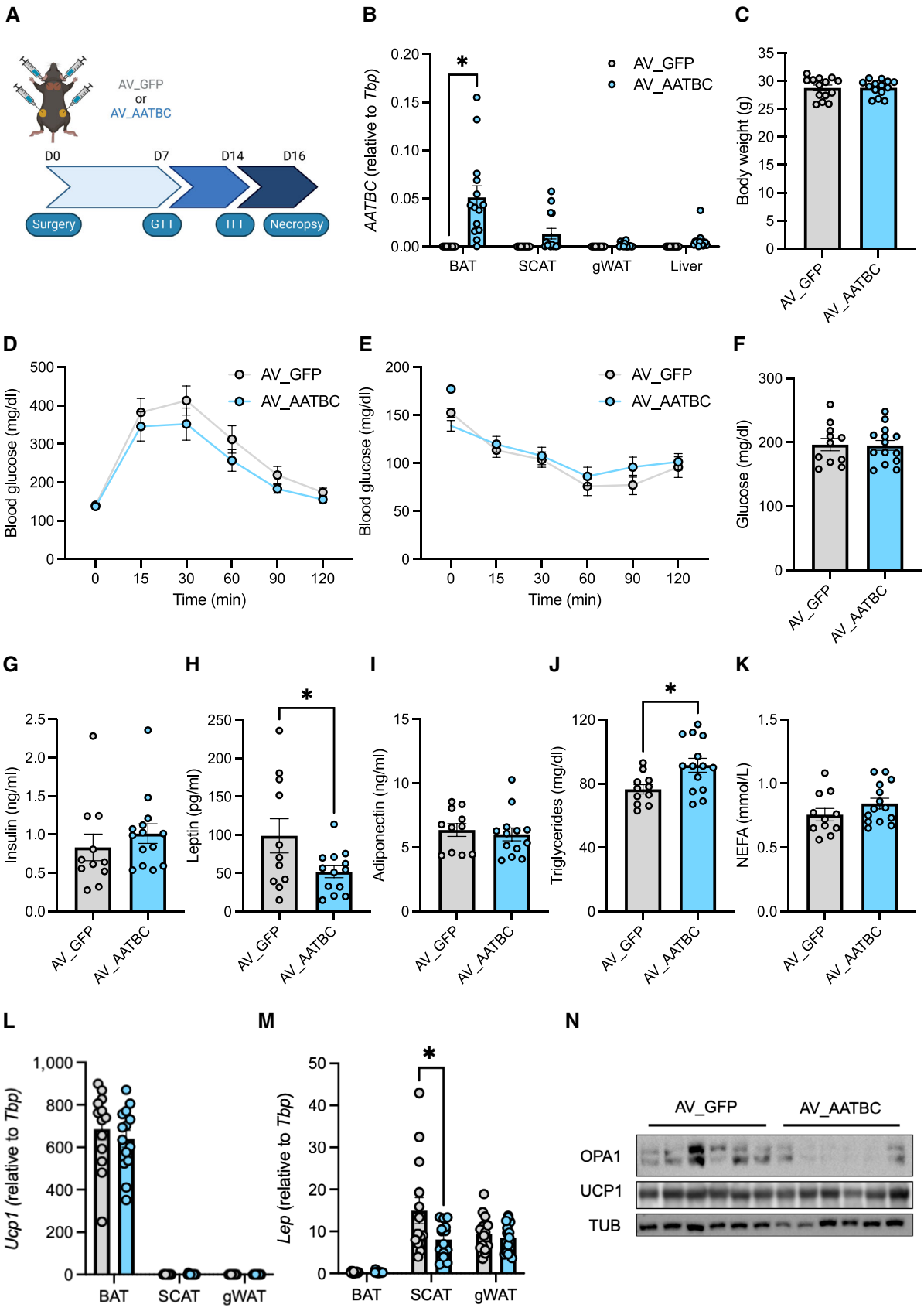

Figure 5.

Figure 5. Expression of human AATBC in mouse adipose tissue impacts metabolism.

A Experimental outline.
B Expression of *AATBC* in adipose tissue depots and liver after injection of AV_GFP or AV_AATBC in brown adipose tissue (BAT) and subcutaneous adipose tissue (scWAT).
C Body weight.
D Glucose tolerance test (GTT).
E Insulin tolerance test (ITT).
F–K Plasma levels of metabolic parameters.
L, M *Ucp1* and *Lep* gene expression in adipose tissue.
B–M $n = 12$ animals per group.
N Immunoblot of OPA1, UCP1, and β-Tubulin of BAT after the specified injections.

Data information: Statistical significance *$P < 0.05$ by 2-way ANOVA followed by Tukey's test (B, L, M) or 2-tailed unpaired Student's *T*-test (C, F–K). Data are presented ± s.e.m.

Expressing human AATBC in mice impacts plasma leptin and triglyceride levels

AATBC is specific to humans, which complicates preclinical *in vivo* investigations in mouse models of metabolic disorders. Regardless, in a first attempt to overcome this obstacle we expressed AATBC in adipose tissue by surgically guided injection of adenovirus (AV) directly into interscapular BAT and inguinal subcutaneous (SCAT) adipose tissue of lean wild-type mice and subsequently performed several metabolic analyses (Fig 5A). In mice that received AATBC-AV, we found marked, localized expression of AATBC lncRNA levels in both BAT and SCAT while in GWAT and liver only minor expression was detectable compared to control injected mice (Fig 5B). While body weight, glucose, and insulin tolerance as well as plasma insulin and adiponectin levels remained unchanged, we observed lower leptin levels (Fig 5C–I). In addition, in mice expressing AATBC, we found higher plasma triglycerides while non-esterified fatty acids levels were unaltered (Fig 5J and K). However, the gene expression levels of *Ucp1* were unaffected (Fig 5L), indicating that the treatment has little to no deleterious effects. In line with the lower plasma leptin levels, also gene expression of leptin (*Lep*) was reduced in scWAT (Fig 5M). In conclusion, our proof-of-concept experiment shows AATBC expression in mouse adipose tissue influences systemic metabolism *in vivo*. Regarding mitochondrial dynamics, we were able to reproduce the *in vitro* finding of a reduction of OPA1 protein levels (Fig 5N).

AATBC is a novel obesity linked human lncRNA

To further corroborate the importance of adipocyte AATBC in systemic metabolism, we investigated the correlation of AATBC with different metabolic parameters in human obesity. Using cross sectional studies with subjects presenting a broad range of body mass index (BMI), we analyzed gene expression of AATBC by qPCR. In two independent cohorts, we found that AATBC was expressed at higher levels in visceral (vis)WAT compared to scWAT (Fig 6A and B). Furthermore, the expression of AATBC was lower in visWAT of obese female subjects compared to lean controls (Fig 6B, D and E), an effect not found in scWAT (Fig 6C and F). In another separate cohort that included mainly obese subjects we were able to perform more in-depth analyses as in addition to anthropomorphic and plasma parameters, RNAseq data from adipose tissue samples was available. We found that AATBC was positively regulated with age and negatively regulated with body weight, body fat and the hip-waist ratio in visWAT of both females and males. Similar to our observation in mice, plasma levels of leptin were inversely correlated with AATBC, whereas adiponectin levels showed no correlation (Fig 6G–L). In line with our previous observations, we found that AATBC was positively correlated with thermogenic markers such as *UCP1* and *PPARG1A* (Fig 7A, B, D and E) and negatively correlated with the expression of genes coding for *ADIPOQ*, *LEP*, *FABP4* and *PPARG* (Fig 7C, F and G–L). These gene expression correlations were also found in scWAT but in the absence of correlations with the metabolic parameters (Appendix Figs S6 and S7). In summary, adipose AATBC is inversely linked to excess adipose tissue and leptin levels as well as correlates with thermogenic markers in humans.

Discussion

Adipocyte plasticity is a key component for the adaptation of metabolism to environmental cues. Thus, the functional features of the adipocyte are matched to the metabolic needs of the organism. This is especially prominent during the adaptation to cold, during which adipocytes adopt a more thermogenic phenotype, or, conversely, when temperature increases or other conditions of positive energy balance such as high-fat diet-induced obesity. If the energy balance

Figure 6. *AATBC* is linked to obesity and leptin levels in humans.

A–C *AATBC* expression in visceral (visWAT) and subcutaneous (scWAT) white adipose tissue grouped by (A) sex (B, C) and body mass index (BMI) ($n = 318$).
D–F *AATBC* expression in visWAT and scWAT of (A) male and female subjects (B, C) lean and obese subjects ($n = 96$ patients).
G, H Correlation matrix of *AATBC* in visWAT of (G) female and (H) male subjects and metabolic parameters (females: $n = 627$, males: $n = 293$).
I–L *AATBC* expression in visWAT of males and females correlated with (I, J) adiponectin and (K, L) leptin plasma levels (I: $\log_e(S) = 11.02$, $P = 0.906$, $\rho_{Spearman} = 0.01$, $CI_{95\%}$ [−0.22, 0.25], $n_{pairs} = 72$, J: $\log_e(S) = 8.91$, $P = 0.465$, $\rho_{Spearman} = 0.12$, $CI_{95\%}$ [−0.22, 0.44], $n_{pairs} = 37$, K: $\log_e(S) = 15.16$, $P = 0.001$, $\rho_{Spearman} = -0.21$, $CI_{95\%}$ [−0.32, −0.09], $n_{pairs} = 267$, L: $\log_e(S) = 12.80$, $P = 0.011$, $\rho_{Spearman} = -0.23$, $CI_{95\%}$ [−0.40, −0.05], $n_{pairs} = 121$).

Data information: Statistical significance *$P < 0.05$ by 2-way ANOVA followed by Tukey's test (A–F). Data is presented with a box containing the 25–75% interval around the median value with whiskers representing the minimum and maximum value.

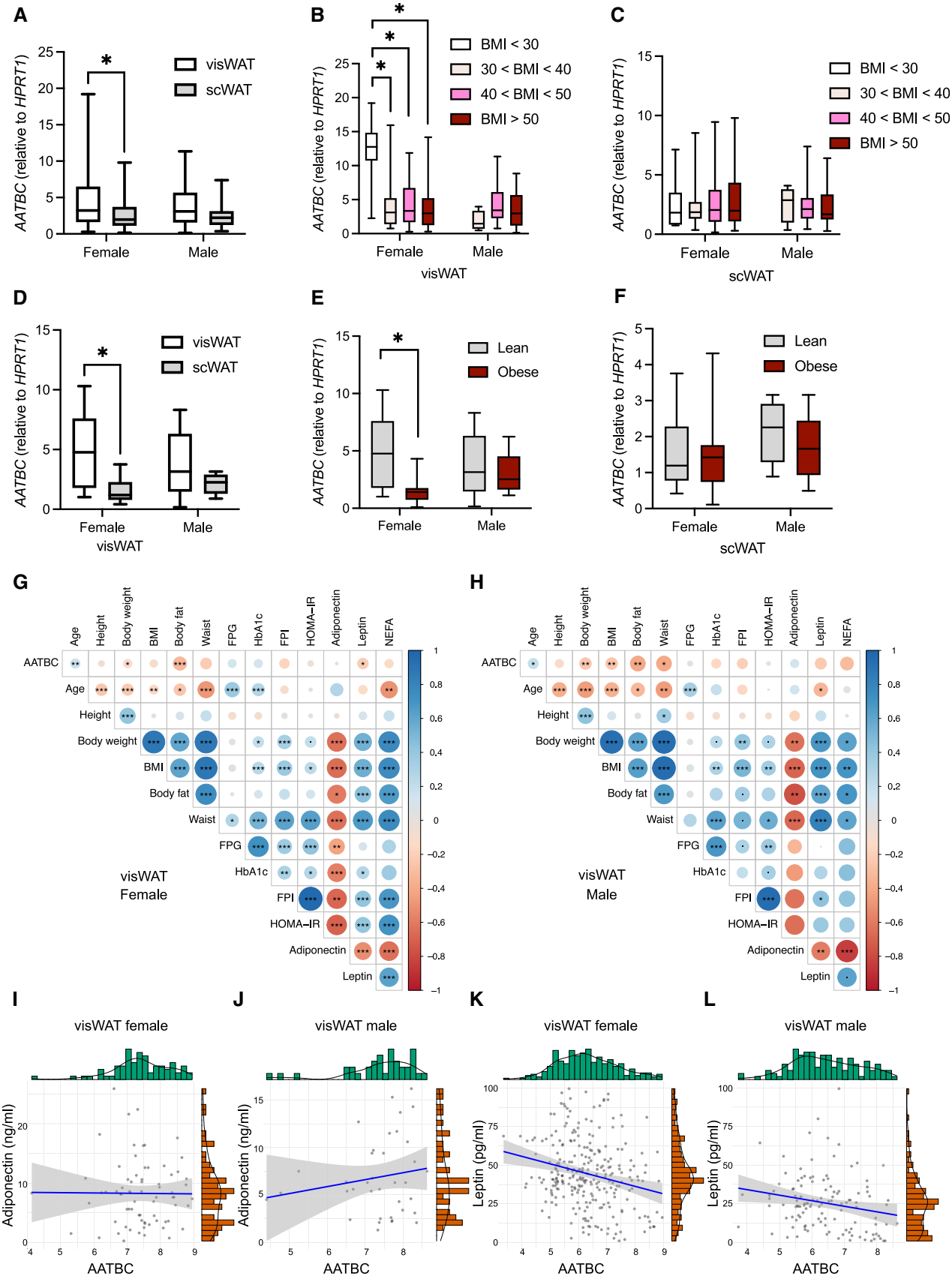

Figure 6.

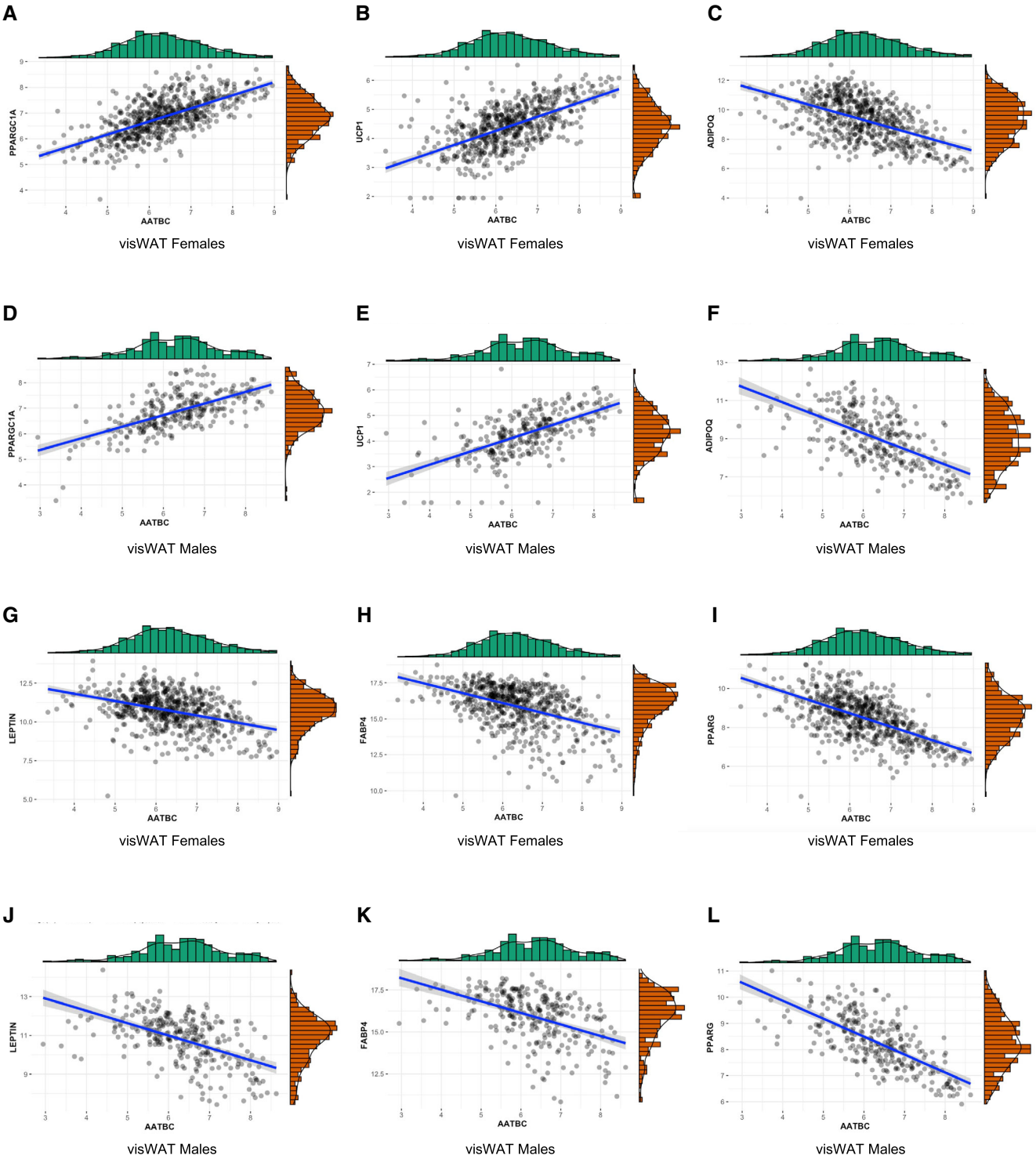

Figure 7. *AATBC* correlates with markers of metabolic health in visceral adipose tissue.

A–L *AATBC* expression correlated with gene expression of the thermogenic markers *PPARGC1A* and *UCP1* and the obesity-related genes *ADIPOQ*, *FABP4*, *LEP* and *PPARG* in visceral adipose tissue of (A–C, G–I) females (n = 627) and (D–F, J–L) males (n = 293) (A: $\log_e(S)$ = 16.47, P = 9.09e^{-78}, $\rho_{Spearman}$ = 0.65, $CI_{95\%}$ [0.61, 0.70]; B: $\log_e(S)$ = 16.63, P = 1.37e^{-60}, $\rho_{Spearman}$ = 0.59, $CI_{95\%}$ [0.54, 0.64]; C: $\log_e(S)$ = 17.94, P = 3.85e^{-43}, $\rho_{Spearman}$ = −0.51, $CI_{95\%}$ [−0.54, −0.45]; D: $\log_e(S)$ = 14.30, P = 1.04e^{-31}, $\rho_{Spearman}$ = 0.61, $CI_{95\%}$ [0.53, 0.68]; E: $\log_e(S)$ = 14.23, P = 7.55e^{-35}, $\rho_{Spearman}$ = 0.64, $CI_{95\%}$ [0.56, 0.70]; F: $\log_e(S)$ = 15.71, P = 6.3e^{-28}, $\rho_{Spearman}$ = −0.58, $CI_{95\%}$ [−0.65, −0.50]; G: $\log_e(S)$ = 17.85, P = 4.95e^{-22}, $\rho_{Spearman}$ = −0.37, $CI_{95\%}$ [−0.44, −0.30]; H: $\log_e(S)$ = 17.89, P = 6.46e^{-29}, $\rho_{Spearman}$ = −0.43, $CI_{95\%}$ [−0.49, −0.36]; I: $\log_e(S)$ = 17.99, P = 7.06e^{-60}, $\rho_{Spearman}$ = −0.59, $CI_{95\%}$ [−0.64, −0.53]; J: $\log_e(S)$ = 15.67, P = 1.1e^{-21}, $\rho_{Spearman}$ = −0.52, $CI_{95\%}$ [−0.60, −0.43]; K: $\log_e(S)$ = 15.65, P = 1.81e^{-19}, $\rho_{Spearman}$ = −0.49, $CI_{95\%}$ [−0.58, −0.40]; L: $\log_e(S)$ = 15.78, P = 2.37e^{-43}, $\rho_{Spearman}$ = −0.69, $CI_{95\%}$ [−0.75, −0.63]).

is positive, whitening prevails over browning and the adipocytes undergo significant morphological and functional remodeling. Here, we show that the obesity-linked lncRNA AATBC is a regulator of adipocyte plasticity that enhances mitochondrial function in human adipocytes.

Mechanistic metabolic studies in humans are challenging and are further complicated if the gene of interest is absent in mice. To overcome these obstacles, we took advantage of hMADS cells which are a representative model of human adipocytes with the potential to switch between white and thermogenic phenotypes and confirmed our findings in primary cells isolated from human WAT and BAT. We demonstrate that in cultured human adipocytes, AATBC stimulates mitochondrial fission, oxygen consumption, and induces the expression of several markers of browning. Its nuclear localization suggests that AATBC exerts its effects by modulation of transcriptional events, but the outcomes of both loss and gain of AATBC function experiments on the global transcriptome were marginal and not linked to changes in genes that would explain the effects of AATBC on mitochondrial function (Chen, 2016). Therefore, a non-transcriptional function for AATBC seems more likely. Indeed, lncRNAs can shuttle out of the nucleus and, for example, LNC00473 has been shown to physically present at the lipid droplet-mitochondrial interface (Tran *et al*, 2020). However, we did not observe such a behavior for AATBC, as it remained strictly nuclear.

Likewise, lipolysis is a key feature of adipocyte function and we found that AATBC influences lipolysis both *in vitro* and *in vivo*. These functional effects were also mirrored in our adipocyte transcriptomic analysis of inhibition and overexpression of AATBC, potentially indicating that AATBC might have a dual role the regulation of adipocyte function. Lipolysis and mitochondrial function are two important pillars of adipocyte plasticity that are rapidly regulated but also change during chronic adaptations to cold or high-fat diet feeding (Weir *et al*, 2018; Dai & Jiang, 2019). To investigate if AATBC is sufficient to alter adipocyte function *in vivo*, we expressed AATBC by a viral strategy in mice where AATBC is naturally absent. We found that AATBC expression altered plasma triglyceride and leptin levels, two important systemic parameters of adipocyte function. One could argue that expressing AATBC in mouse adipocyte might be artificial, as AATBC is a human lncRNA and could be non-functional in a mouse cell. However, it has been shown that expressing human lncRNAs in mice is useful for investigating lncRNA function (Ruan *et al*, 2020) and we did not observe any adverse side effects in mice expressing AATBC. While more work is certainly needed to study the role of AATBC in non-shivering thermogenesis and/or obesity, ideally using a stable transgenic mouse model, our work here indicates that adipocyte AATBC plays role in systemic metabolism.

We investigated the expression pattern of AATBC in adipose tissue in three separate human cohorts. As inter-individual variation is bigger in humans than in mice, one needs to keep in mind the limitations of human correlation studies. Confounding factors in our obese patients could be comorbidities and medication. Therefore, we used big cohort sizes to level out such influences. In humans, adipose AATBC expression is correlated with a thermogenic phenotype. This was also reflected in human primary adipocytes and hMADS cells. Regardless, AATBC is more expressed in visWAT compared to scWAT both in lean and obese patients, which is in line with the observation of an inverted pattern of thermogenic gene expression in those adipose depots of humans compared to mice (Zuriaga *et al*, 2017). In line with this notion, AATBC expression was correlated inversely with parameters of obesity and plasma leptin levels. Also, in our mouse model plasma leptin levels were inversely correlated with AATBC expression but we do not expect the range of the observed changes in plasma leptin levels to immediately affect satiety and body weight regulation. Mitochondrial dynamics are equally important for proper white adipocyte function, as patients with mutations in *MFN2* display a fragmented mitochondrial network, excess adiposity, and paradoxical suppression of leptin expression (Rocha *et al*, 2017). In general, proper mitochondrial dynamics are critical for maintaining a healthy pool of mitochondria and efficient mitophagy (Liesa & Shirihai, 2013). To this end, it will be intriguing to study the role of AATBC in obesity-induced mitochondrial dysfunction, in adipocyte and potentially also other cell types as AATBC expression is not restricted to adipocytes. In conclusion, our study identifies AATBC as a novel lncRNA linked to adipocyte function and obesity with the potential to manipulate mitochondrial function and thermogenic plasticity in humans.

Materials and Methods

Cell culture

Human SVF (RNAseq screening, Fig 1)

Human primary adipose-derived stem cells (hpASCs) were isolated and stimulated as previously described (Higareda-Almaraz *et al*, 2018). In brief, subcutaneous lipoaspirates from healthy female donors (n = 4) were thawed, cultivated in EGM-2 Medium (Lonza), and used after 1–3 passages. 2 days after the cells reached confluency (= day 0), adipocyte differentiation was induced with the following medium (DMEM/Ham's F12 [50:50]; supplemented with 5 mM HEPES, 2 mM L-glutamine, 100 µg/ml normocin, 860 nM insulin, 10 µg/ml apo-transferrin, 100 nM rosiglitazone, 0.2 nM triiodothyronin) supplemented with 100 µM 3-isobutyl-1-methylxanthine (IBMX), and 1 µM dexamethasone (Dex). At day 7 of differentiation, supplementation with insulin was stopped. At day 9 of differentiation, the differentiated adipocytes were stimulated with 1 µM norepinephrine (NE; dissolved in 10 mM HCl) or vehicle (VE, 10 mM HCl) for 3 h.

hMADS cells

Human multipotent adipose derived stem (hMADS) cells were cultured as previously described (Giroud *et al*, 2021). Briefly, cells were kept until confluency in proliferation medium (Dulbecco's Modified Eagle's Medium [DMEM]), (Lonza, Switzerland # BE12-707F) supplemented with 10% FBS (Sigma, Germany), 10 mmol/l 4-(2-hydroxyethyl)-1-piperazineethanesulfonic acid (HEPES; Gibco, Germany #15630056), 2.5 ng/ml human fibroblast growth factor-basic (hFGF2) (PeproTech, Germany #100-18B), 50 mg/ml penicillin, and 50 mg/ml streptomycin (Gibco, Germany #15140122), followed by 48 h of incubation without hFGF2. The induction of the differentiation towards adipocytes was started (d0) using a cocktail of DMEM/Ham's F12 (Lonza, Switzerland # BE12-615F) supplemented with 10 mg/ml apo-transferrin (Sigma, Germany # T1428), 10 nM insulin (Sigma, Germany # I 9278), 100 nM rosiglitazone (Cayman, Germany #71740), 0.2 nM triiodothyronine (T3) (Sigma, Germany #6893-02-3), 1 mmol/l dexamethasone (DEX) (Sigma, Germany #

D4902), 1 mM 3-isobutyl-1-methylxanthine (IBMX) (Sigma, Germany #28822-58-4). After 48 h the induction medium was replaced by the differentiation medium containing DMEM/Ham's F12, 10 mg/ml transferrin, 10 nM insulin, 0.2 nM triiodothyronine and 1 μM rosiglitazone. Until day 9, the medium was changed every other days. At day 9, thermogenic (referred to as "Thermo") differentiated hMADS cells were obtained with chronic rosiglitazone treatment until day of completion of the experiment (d14) whereas a whiter phenotype was achieved by removal of rosiglitazone (referred to as "White").

Human SVF purification and differentiation

Human stromal vascular fraction was purified from subcutaneous adipose tissue from patients undergoing abdominoplasty. The study was approved by the ethical committee (vote no. 300/16) of the University of Ulm after written informed consent. Minced tissue was chemically digested using collagenase (Sigma, Germany #11088793001) in BSA (Sigma, Germany #A8806-5G) media (ratio 1:3) for 30–45 min until the digestion was stopped by the addition of FBS (Sigma, Germany) at a 10% v/v ratio. To purify primary adipocytes from of the digested tissue, the mixture was first filtered consecutively through 100, 70 and 48 μm meshes and then centrifugated to finally separate the primary adipocytes in the pellet from the supernatant. Cells were plated and treated like hMADS cells.

Human SVF purification and differentiation (refers to Fig 2A and B)

Preadipocytes isolated from the supraclavicular and abdominal subcutaneous region were cultured, differentiated, and stimulated as previously described (Jespersen *et al*, 2013). RNA was extracted from adipocytes using the TRIzol method. RNA sequencing was performed by BGI (Hong Kong) using 1,000 ng RNA for the TruSeq cDNA library construction (Illumina). 3Gb data was generated per sample on a HiSeq 2000 sequencer (Illumina) and a 91-paired end sequencing strategy was used. Read quality was assessed using FastQC (http://www.bioinformatics.babraham.ac.uk) and the following pre-processing steps where performed using the Fastx toolkit (http://hannonlab.cshl.edu) and PRINSEQ: 7 nt were clipped off from the 5′-end of every read (Schmieder & Edwards, 2011). The reads were then filtered to remove all N-reads. The 3′-ends were then trimmed, and the reads filtered to minimum Q25 and 50 bp length. Reads were then mapped with tophat2 to the human genome GRCh38 Ensembl release 77. Read counts were imported into R, and DESeq2 was used for identifying differential expression.

Modulation of gene expression

The expression of *AATBC* was modulated *in vitro* using antisense oligonucleotide-mediated knockdown (ASO, Exiqon, #634048-6, #634048-4), siRNA-mediated knockdown (Lincode Human AATBC [Horizon Discovery, #284837]) and adenovirus (AV) mediated overexpression (VectorBuilder, #AVM (VB150925-10024) + GFP). White hMADS were transfected at day 12 of differentiation with 30 nmol of siRNA or ASO at day 10 using Lipofectamine™ RNAiMAX transfection reagent (Thermo Scientific, #13778075) according to the manufacturer's protocol. For overexpression, white hMADS cells were infected with 200 particles of virus per cell. 24 h later, the transfection medium was removed and replaced by the suitable differentiation medium. 48 h after transfection cells were harvested.

Nuclear RNA extraction

Nuclear RNA was purified using a Cytoplasmic & Nuclear RNA Purification Kit (Norgen, Canada # 21000) according to the manufacturer's instructions. cDNA was synthesized with Maxima™ H Master Mix 5× (Thermo Fisher Scientific, #M1661), followed by qPCR according to the PowerUp™ SYBR Green technology (Applied Biosystems, #A25741).

Immunoblot

Protein expression was investigated using Western blot as described previously (Giroud *et al*, 2021). Cells were lysed in RIPA buffer (150 mM NaCl, 5 mM EDTA, 50 mM Tris pH 8, 0.1% w/v SDS, 1% w/v IGEPAL® CA-630, 0.5% w/v sodium deoxycholate) containing protease inhibitors (Sigma) in a 1:100 v/v ratio. Protein concentrations of the lysates were determined using Pierce BCA Protein Assay (Thermo Scientific) following the manufacturer's protocol. 30 μg of total protein were loaded per well on Bolt™ 4–12% Bis-Tris gels (Thermo Scientific, #NW04120BOX) and blotted on a 0.2 μm PVDF membrane (Bio-Rad, #1704156) using the Trans-Blot® Turbo™ system. Membranes were incubated in primary antibodies at a dilution of 1:1,000 v/v in ROTI-Block (Roth, Germany #A151.1) after blocking in ROTI-Block. Secondary antibody (concentration of 1:10,000 v/v in ROTI-Block) incubation was performed for 1 h at room temperature. All antibodies used are shown in Table 1. After antibody incubation membranes were washed 4× for 10 min in TBS-T (Tween 0.1%). Bands were detected using a Chemidoc MP System (Bio-Rad, #1704156).

Gene expression analysis

RNA of cells and tissues were extracted using TRIzol (Invitrogen, #15596026) and NucleoSpin® RNA kit (Macherey-Nagel, #740955.250) according to the manufacturer's instruction. cDNA was synthesized with Maxima™ H Master Mix 5× (Thermo Scientific, #M1661), followed by qPCR according to the PowerUp™ SYBR Green technology (Applied Biosystems, #A25741) using the primers listed in Table 2. Gene expression was calculated using the $\Delta\Delta C_t$-method normalized to the housekeeping gene indicated in the respective figure.

Oil-Red-O staining

Cells were fixed using 8% paraformaldehyde (Sigma). After washing with 60% isopropanol cells were stained with a 60/40 v/v mixture of ORO (Sigma) and H_2O for 10 min at room temperature. After

Table 1. Antibodies.

Mfn2	ab56889 (Abcam)
OXPHOS	ab110413 (Abcam)
Opa1	ab42364 (Abcam)
β-tubulin	2146S (Cell Signaling Technology)
TOMM20	ab78547 (Abcam)
Anti-rabbit IgG	7074S (Cell Signaling Technology)
Anti-mouse IgG	7076S (Cell Signaling Technology)

Table 2. Primers.

h_PLIN1_F	ACCCCCCTGAAAAGATTGCTT
h_PLIN1_R	GATGGGAACGCTGATGCTGTT
h_TBP_F	ACGCCAGCTTCGGAGAGTTC
h_TBP_R	CAAACCGCTTGGGATTATATTCG
h_UCP1_F	CTGGACACGGCCAAAGTC
h_UCP1_R	GGACACCTTTATACCTAATAACACTGG
m_Ucp1_F	AGGCTTCCAGTACCATTAGGT
m_Ucp1_R	CTGAGTGAGGCAAAGCTGATTT
m_Tbp_F	AGAACAATCCAGACTAGCAGCA
m_Tbp_R	GGGAACTTCACATCACAGCTC
m_Adipoq_F	GGAGAGAAAGGAGATGCAGGT
m_Adipoq_R	CTTTCCTGCCAGGGGTTC
h_ADIPOQ_F	GCTGGTCTGAAACTCCTGACA
h_ADIPOQ_R	CGGGCAGAGCTAATAGCAGTA
h_AATBC_F	ACCGGGCAAATCTGAAACCA
h_AATBC_R	CGTTGATAACCGGCCTTCCT
h_12S_F	CCTGGTCATGAACAAGCAATACC
h_12S_R	GTGTCTGGCTAGTGAGGACTG
h_U1_F	ATACTTACCTGGCAGGGGAG
h_U1_R	CAGGGGAAAGCGCGAACGCA
h_FABP4_F	CCTTTAAAAATACTGAGATTTCCTTCA
h_FABP4_R	GGACACCCCCATCTAAGGTT
h_NADH_F	GAGCGATGGTGAGAGCTAAGGT
h_NADH_R	CCCTAAAACCCGCCACATCT
m_Lep_F	CAGGATCAATGACATTTCACACA
m_Lep_R	GCTGGTGAGGACCTGTTGAT
h_LPL_F	TTCTGGATTCCAATGCTTCGA
h_LPL_R	CGAGTCGTCTTTCTCCTGATGAT

washing imaging was performed. Quantification of the staining was performed after elution of the dye using 100% isopropanol and measurement of absorbance at 500 nm.

Analysis of mitochondrial respiration

To assess mitochondrial respiration a Seahorse XFe24 device (Agilent # 102238-100, S7801A) was used. hMADS cells were seeded differentiated and transfected or transduced at day 12 as described above. Oxygen consumption rate was determined during a Mito Stress Test (All Sigma-Aldrich: 1 μM Oligomycin-A [#75351], 1.2 μM FCCP [#C2920], 2 μM Rotenone [#R8875], 2 μM Antimycin A [#A8674]) with additional treatment with Isoproterenol (100 nM, #I5627-5G).

Quantification of mitochondrial DNA

To assess cellular mitochondrial amount, DNA was extracted using a DNA Extraction Kit (Macherey-Nagel, #740952.50) and used for qPCR as described before (Giroud *et al*, 2016). The expression of the mitochondrial gene *NADH* was normalized to the single copy nuclear gene *LPL*.

In situ hybridization—RNAscope®

To visualize the intracellular localization of ATTBC, we used the RNAscope® Multiplex Fluorescent Reagent Kit v2- Hs (ACD Bio, #323135). Undifferentiated hMADS cells were seeded on coverslips in 24-well tissue culture dishes, grown to confluence and differentiated into thermogenic adipocytes for 12 days (see hMADS cells differentiation). *In situ* hybridization was performed according to the manufacturer's protocol (Advanced Cell Diagnostics), using a probe designed to specifically detect human AATBC (RNAscope® Probe Hs-AATBC [Advanced Cell Diagnostics, #519681]), in combination with the Opal 620 Fluorophore Reagent (Akoya Biosciences). Cells were visualized on a Leica TCS SP5 confocal microscope (Leica, Germany). Images were acquired for all conditions as z-stacks (steps of 0.5 μm along the z axis) with a glycerol-based immersion fluid-immersed 63× objective. Acquisition parameters were kept consistent for all images. The same image processing was performed using ImageJ (FIJI) software for the different conditions.

Mitochondria 3D reconstruction and morphometric analysis

Immunofluorescence was performed at day 14 of differentiation as previously described (Pisani *et al*, 2018). To visualize the mitochondrial network TOMM20 antibody (Abcam, #ab78547, 1:1,000 v/v) was used followed by incubation with a fluorescent antibody (molecular probes, A-21429, 1:1,000 v/v). Immunofluorescent samples were analyzed using a Laser Scanning Confocal Microscope (Olympus Fluoview 1200, Olympus, Tokyo, Japan) equipped with an Olympus UPlanSApo 60 × 1.35 and an UplanSApo 40 × 1.25Sil Oil immersion objective (Olympus, Tokyo, Japan) at a resolution of app. 100 μm/pixel (60×) and 600 nm step size. For mitochondrial 3D reconstruction, images were deconvolved using the FIJI plugins point spread function (PSF) generator (Kirshner *et al*, 2013) and DeconvolutionLab (Sage *et al*, 2017). Z-step was set to 0.6 μm and a PSF algorithm (Born & Wolf 3D Optical model) was used for PSF generation, as previously described (Seitz *et al*, 2019). The generated PSF and a 3D deconvolution algorithm (Richardson-Lucy with TV regularization) were applied to microscopic images using DeconvolutionLab. From the deconvolved 2D and 3D binary images (8-bit images), mitochondrial network was determined by generating a skeleton of the images using the Fiji plugin Skeletonize3D and analyzed using the plugin AnalyzeSkeleton (2D/3D). This plugin tags all pixel/voxels in a skeleton image and then counts the junctions and branches of the mitochondrial network and measures their average length. For mitochondrial network analysis, minimum of 20 cells were analyzed.

Mouse experiments

Animal experiments were performed in accordance with German animal welfare legislation and approved by the state ethics committee and government of Upper Bavaria (no. ROB-55.2-2532.Vet_02-17-125). We followed the ARRIVE guidelines (Percie du Sert *et al*, 2020). Mice were group-housed at 22°C with a 12 h dark–light cycle in the animal facility of Helmholtz Center Munich. 9-week-old male C57BL/6J mice were purchased from Janvier Labs and acclimatized in the Helmholtz center facility for 3 weeks. Induction of anesthesia was performed using 4% isoflurane and upheld by inhalation of 2% isoflurane. Incisions were made over the intrascapular

brown adipose tissue and inguinal adipose tissue. Injections of 25 µl containing 4×10^7 viral particles of AV_AATBC or control were performed into each lobe of the tissues in a randomized fashion. Experiments were performed not blinded. Exclusion criteria were suboptimal surgical recovery. For glucose tolerance test (GTT), performed at day 7 and insulin tolerance test (ITT), performed at day 14, mice were fasted for 6 h after which they received intraperitoneal injections of glucose (3 g/kg for GTT) and insulin (0.7 U/kg for ITT). Blood glucose was measured from the tail vein at 15, 30, 60, 90, and 120 min after injection. After 12 days mice were euthanized using cervical dislocation and necropsy was performed. Plasma was analyzed for metabolic parameters including adiponectin, triglycerides, and non-esterified fatty acids using a serum analyzer (AU480 Beckman Coulter). Plasma levels of leptin and insulin were assessed using ELISAs according to the manufacturer's instructions (R&D Systems, #MOB00B & Crystal Chem, #90082, respectively).

Human data

Human adipose tissue samples (RNAseq screening, refers to Fig 1)

Human BAT and WAT were removed from the same incision site in the supraclavicular localization, BAT being fluorodeoxyglucose-positron emission tomography (FDG-PET)-positive scan sites and WAT being not. The Study protocol was approved by the ethics committee of the Hospital District of Southwestern Finland, and subjects provided written informed consent following the committee's instructions. The study was conducted according to the principles of the Declaration of Helsinki. All potential subjects who donated BAT were screened for metabolic status, and only those with normal glucose tolerance and normal cardiovascular status (as assessed based on electrocardiograms and measured blood pressure) were included. The age range of the subjects was 23–49 years. We studied a group of five healthy volunteers (three females, two males).

Human samples (RNAseq, refers to Figs 6 and 7)

The acquisition of human data from cohorts 1 and 2 has been previously described (Giroud *et al*, 2021). Briefly, cohort 1 includes 318 individuals (249 female individuals, 69 male individuals; BMI range: 21.9–97.3 kg/m^2, age range: 19–75 years) undergoing elective laparoscopic surgery during which subcutaneous (scWAT) and visceral, omental (visWAT) adipose depots were obtained. Cohort 2 and 3 are from the Leipzig Obesity Biobank. Cohort 2 includes 96 individuals (23 lean female individuals, mean age 43.3 ± 7.4 years, mean BMI 23.7 ± 1.3 kg/m^2, 48 obese female individuals, mean age 42.9 ± 8.3 years, mean BMI 45.9 ± 6.1 kg/m^2, 9 lean male individuals, mean age 44.7 ± 7.1 years, mean BMI 22.3 ± 1.8 kg/m^2, and 16 obese male individuals, mean age 42.2 ± 7.6 years, mean BMI 44.9 ± 5.2 kg/m^2). Cohort 3 comprises 1,415 individuals, with visWAT samples collected from 920 individuals (female lean [n = 45, mean age 62.1 ± 13.7 years, mean BMI 24.4 ± 2.9 kg/m^2], female obese [n = 582, mean age 46.1 ± 11.8 years, mean BMI 48.5 ± 8.5 kg/m^2], male lean [n = 44, mean age 61.4 ± 15.7 years, mean BMI 24.9 ± 3.5 kg/m^2], and male obese [n = 249, mean age 48.2 ± 11.7 years, mean BMI 49.1 ± 8.5 kg/m^2]) and scWAT samples taken from 814 individuals (female lean [n = 33, mean age 63.8 ± 12.9 years, mean BMI 24.7 ± 2.8 kg/m^2], female obese [n = 545, mean age 46.7 ± 12.0 years, mean BMI 48.3 ± 9.2 kg/m^2], male lean [n = 25, mean age 65.6 ± 14.3 years, mean BMI 25.5 ± 2.6 kg/m^2], and male obese [n = 211, mean age 48.09 ± 12.4 years, mean BMI 49.5 ± 8.0 kg/m^2]). Patients were classified as lean when their BMI was < 30 kg/m^2. For cohort 3, human single-end and rRNA-depleted RNA-seq data were prepared with a SMARTseq protocol (Picelli *et al*, 2014; Song *et al*, 2018). In brief, RNA was enriched and reverse transcribed by Oligo(dT) and TSO primers. cDNA was amplified by ISPCR primers and processed with Tn5 using Nextera DNA Flex kit. All libraries were sequenced on an Novaseq 6000 instrument at Functional Genomics Center Zurich (FGCZ). Approval for all three studies was obtained from the Ethics Committee of the University of Leipzig (approval no: 159-12-21052012) before the study and acquisition was performed in accordance with the declaration of Helsinki.

Bioinformatic analysis

Bioinformatic analysis (RNAseq screening, refers to Fig 1)

RNA quality was assessed using BioAnalyzer 2100 (Agilent); all samples had RIN values ≥ 8.5. 4 µg total RNA per sample were used for the TruSeq Stranded mRNA LT Sample Prep Kit (Illumina) to generate cDNA libraries according to the manufacturer's protocol. Single read sequencing was carried out using Illumina/Solexa HiSeq 2000. High-throughput sequencing was conducted by the Biomedical Sequencing Facility, Vienna. RNAseq alignment, long non-coding quantification and differential expression analysis were performed as follows: Raw sequencing reads were aligned against the human hg38 genome using STAR aligner with default parameters (Dobin & Gingeras, 2015). The mapped reads were assigned to genes using featureCount from the Bioconductor package Rsubread (Liao *et al*, 2014). All annotated lncRNAs were quantified across each condition, using hg38 annotation. Normalization and differential expression analysis were performed using the R/Bioconductor package DESeq2 (Love *et al*, 2014). Significance was assumed for an adjusted P-value < 0.01. Data of the hpAS treated with norepinephrine are publicly available sequencing data (Tran *et al*, 2020).

Bioinformatic analysis (RNAseq human cohort 3, refers to Figs 6 and 7)

Adapters and low quality bases of raw reads were trimmed using fastp v0.20.0 (Chen *et al*, 2018). Only reads with a minimum read length of 18 nts and which surpass a quality cut-off of 20 were kept. The remaining reads were aligned against the human (GRCh38.p13) genome from GENCODE (Frankish *et al*, 2019) applying the STAR alignment algorithm v2.7.4a (Dobin *et al*, 2013), allowing 50 multiple alignments per read. Standard pre- and post-mapping quality control was computed using FASTQC v.0.11.4 (https://www.bioinformatics.babraham.ac.uk). Gene counts were conducted with featureCounts v2.0.1 (https://subread.sourceforge.net) where multiple mapped reads were fractionally counted. Count data were homoscedastic normalized with respect to library size using the variance stabilizing transformation from DESeq2 v1.32.0 (Love *et al*, 2014). Correlation analyses were computed using the psych R package v2.1.6 with the spearman correlation coefficient and confidence intervals of 0.05. P-values were adjusted using the Holm's method (http://www.jstor.org/stable/4615733). Visualization of correlation analysis was performed with the corrplot v0.90 and ggstatsplot v0.8.0 R packages under R version 4.1.

Statistics

Data is presented as mean ± standard error of mean (s.e.m.). Student's *t*-test and 2-way ANOVA were used as indicated in the figure legends and performed using GraphPad Prism 9.0 and R 4.1.0. No sample size calculation was performed. *In vitro* experiments were performed at least 3 times and pooled where possible. Differences were deemed significant with a *P*-value < 0.05 and indicated by an asterisk.

Data availability

The RNAseq data of human adipose tissue have been deposited at the GEO repository accession number GSE239673 (https://www.ncbi.nlm.nih.gov/geo/query/acc.cgi?acc=GSE236966). Human primary cells RNAseq have been published previously (Tran *et al*, 2020). The human obesity datasets of the Leipzig Obesity BioBank (Figs 6 and 7) are not publicly available due to concerns regarding participant/patient anonymity. Requests to access the datasets should be directed to Matthias Blüher. RNAseq data of the AATBC manipulation have been deposited at the GEO repository, accession number GSE236966 (http://www.ncbi.nlm.nih.gov/geo/query/acc.cgi?acc=GSE236966).

Expanded View for this article is available online.

Acknowledgements
We thank Ez-Zoubir Amri (Institut de Biologie Valrose, Université Nice Sophia Antipolis, France) for sharing hMADS cells. We thank Daniela Hass for outstanding technical support as well as Florian Pauler for valuable advice on the RNAseq analysis. We thank Florian Pauler for assistance with the RNAseq analysis. We thank the members of Bartelt Lab for enjoyable atmosphere and stimulating discussions. The figures were created using BioRender. MG was supported by an Alexander von Humboldt Foundation postdoctoral fellowship. PF-P was supported by the Deutsche Forschungsgemeinschaft (FI 1700/7-1, Heisenberg program). DT was supported by a grant from the German Research Association (TE912/2-2). SH was supported by the Helmholtz Future topic 'Aging and Metabolic Programming, AMPro', by the Deutsche Forschungsgemeinschaft Trans-Regio (TRR205) and the Deutsches Zentrum für Herz-Kreislauf-Forschung Standortprojekt Cardiometabolism. AB was supported by the Deutsche Forschungsgemeinschaft Sonderforschungsbereich 1123 (B10), the Deutsches Zentrum für Herz-Kreislauf-Forschung Junior Research Group Grant, and the European Research Council (ERC) Starting Grant PROTEOFIT. We apologize to colleagues whose work we could not cite due to space limitations. Open Access funding enabled and organized by Projekt DEAL.

Author contributions
Maude Giroud: Conceptualization; data curation; formal analysis; investigation; visualization; methodology; writing – original draft; project administration; writing – review and editing. **Stefan Kotschi:** Conceptualization; data curation; formal analysis; investigation; visualization; methodology; writing – original draft; project administration; writing – review and editing. **Yun Kwon:** Data curation; formal analysis; writing – review and editing. **Ophélia Le Thuc:** Data curation; formal analysis; writing – review and editing. **Anne Hoffmann:** Data curation; formal analysis; writing – review and editing. **Manuel Gil-Lozano:** Data curation; formal analysis; writing – review and editing. **Michael Karbiener:** Data curation; formal analysis; writing – review and editing. **Juan Carlos Higareda-Almaraz:** Data curation; formal analysis; writing – review and editing. **Sajjad Khani:** Data curation; formal analysis; writing – review and editing. **Daniel Tews:** Data curation; formal analysis; writing – review and editing. **Pamela Fischer-Posovszky:** Data curation; formal analysis; writing – review and editing. **Wenfei Sun:** Data curation; formal analysis; writing – review and editing. **Hua Dong:** Data curation; formal analysis; writing – review and editing. **Adhideb Ghosh:** Data curation; formal analysis; writing – review and editing. **Christian Wolfrum:** Data curation; formal analysis; writing – review and editing. **Martin Wabitsch:** Data curation; formal analysis; writing – review and editing. **Kirsi A Virtanen:** Data curation; formal analysis; writing – review and editing. **Matthias Blüher:** Data curation; formal analysis; writing – review and editing. **Søren Nielsen:** Data curation; formal analysis; writing – review and editing. **Anja Zeigerer:** Data curation; formal analysis; writing – review and editing. **Cristina García-Cáceres:** Data curation; formal analysis; writing – review and editing. **Marcel Scheideler:** Data curation; formal analysis; writing – review and editing. **Stephan Herzig:** Conceptualization; supervision; funding acquisition; writing – original draft; project administration; writing – review and editing. **Alexander Bartelt:** Conceptualization; supervision; funding acquisition; writing – original draft; project administration; writing – review and editing.

Disclosure and competing interests statement
The authors declare that they have no conflict of interest.

References

Alvarez-Dominguez JR, Bai Z, Xu D, Yuan B, Lo KA, Yoon MJ, Lim YC, Knoll M, Slavov N, Chen S *et al* (2015) *De novo* reconstruction of adipose tissue transcriptomes reveals long non-coding RNA regulators of brown adipocyte development. *Cell Metab* 21: 764 – 776

Anunciado-Koza R, Ukropec J, Koza RA, Kozak LP (2008) Inactivation of UCP1 and the glycerol phosphate cycle synergistically increases energy expenditure to resist diet-induced obesity. *J Biol Chem* 283: 27688 – 27697

Bai Z, Chai XR, Yoon MJ, Kim HJ, Lo KA, Zhang ZC, Xu D, Siang DTC, Walet ACE, Xu SH *et al* (2017) Dynamic transcriptome changes during adipose tissue energy expenditure reveal critical roles for long noncoding RNA regulators. *PLoS Biol* 15: e2002176

Bartelt A, Heeren J (2014) Adipose tissue browning and metabolic health. *Nat Rev Endocrinol* 10: 24 – 36

Bartelt A, Bruns OT, Reimer R, Hohenberg H, Ittrich H, Peldschus K, Kaul MG, Tromsdorf UI, Weller H, Waurisch C *et al* (2011) Brown adipose tissue activity controls triglyceride clearance. *Nat Med* 17: 200 – 205

Bartelt A, John C, Schaltenberg N, Berbee JFP, Worthmann A, Cherradi ML, Schlein C, Piepenburg J, Boon MR, Rinninger F *et al* (2017) Thermogenic adipocytes promote HDL turnover and reverse cholesterol transport. *Nat Commun* 8: 15010

Bartelt A, Widenmaier SB, Schlein C, Johann K, Goncalves RLS, Eguchi K, Fischer AW, Parlakgul G, Snyder NA, Nguyen TB *et al* (2018) Brown adipose tissue thermogenic adaptation requires Nrf1-mediated proteasomal activity. *Nat Med* 24: 292 – 303

Bast-Habersbrunner A, Kiefer C, Weber P, Fromme T, Schiessl A, Schwalie PC, Deplancke B, Li Y, Klingenspor M (2021) LncRNA Ctcflos orchestrates transcription and alternative splicing in thermogenic adipogenesis. *EMBO Rep* 22: e51289

Becher T, Palanisamy S, Kramer DJ, Eljalby M, Marx SJ, Wibmer AG, Butler SD, Jiang CS, Vaughan R, Schoder H *et al* (2021) Brown adipose tissue is associated with cardiometabolic health. *Nat Med* 27: 58 – 65

Berbee JF, Boon MR, Khedoe PP, Bartelt A, Schlein C, Worthmann A, Kooijman S, Hoeke G, Mol IM, John C *et al* (2015) Brown fat activation reduces hypercholesterolaemia and protects from atherosclerosis development. *Nat Commun* 6: 6356

Boutant M, Kulkarni SS, Joffraud M, Ratajczak J, Valera-Alberni M, Combe R, Zorzano A, Canto C (2017) Mfn2 is critical for brown adipose tissue thermogenic function. *EMBO J* 36: 1543 – 1558

Cannon B, Nedergaard J (2011) Nonshivering thermogenesis and its adequate measurement in metabolic studies. *J Exp Biol* 214: 242 – 253

Chen LL (2016) Linking long noncoding RNA localization and function. *Trends Biochem Sci* 41: 761 – 772

Chen S, Zhou Y, Chen Y, Gu J (2018) fastp: an ultra-fast all-in-one FASTQ preprocessor. *Bioinformatics* 34: i884 – i890

Chondronikola M, Volpi E, Borsheim E, Porter C, Annamalai P, Enerback S, Lidell ME, Saraf MK, Labbe SM, Hurren NM *et al* (2014) Brown adipose tissue improves whole-body glucose homeostasis and insulin sensitivity in humans. *Diabetes* 63: 4089 – 4099

Dai W, Jiang L (2019) Dysregulated mitochondrial dynamics and metabolism in obesity, diabetes, and cancer. *Front Endocrinol (Lausanne)* 10: 570

Dallner OS, Marinis JM, Lu YH, Birsoy K, Werner E, Fayzikhodjaeva G, Dill BD, Molina H, Moscati A, Kutalik Z *et al* (2019) Dysregulation of a long noncoding RNA reduces leptin leading to a leptin-responsive form of obesity. *Nat Med* 25: 507 – 516

Ding C, Lim YC, Chia SY, Walet ACE, Xu S, Lo KA, Zhao Y, Zhu D, Shan Z, Chen Q *et al* (2018) *De novo* reconstruction of human adipose transcriptome reveals conserved lncRNAs as regulators of brown adipogenesis. *Nat Commun* 9: 1329

Dobin A, Gingeras TR (2015) Mapping RNA-seq reads with STAR. *Curr Protoc Bioinformatics* 51: 11.14.11 – 11.14.19

Dobin A, Davis CA, Schlesinger F, Drenkow J, Zaleski C, Jha S, Batut P, Chaisson M, Gingeras TR (2013) STAR: ultrafast universal RNA-seq aligner. *Bioinformatics* 29: 15 – 21

Eisenberg E, Levanon EY (2013) Human housekeeping genes, revisited. *Trends Genet* 29: 569 – 574

Frankish A, Diekhans M, Ferreira AM, Johnson R, Jungreis I, Loveland J, Mudge JM, Sisu C, Wright J, Armstrong J *et al* (2019) GENCODE reference annotation for the human and mouse genomes. *Nucleic Acids Res* 47: D766 – D773

Giacomello M, Pyakurel A, Glytsou C, Scorrano L (2020) The cell biology of mitochondrial membrane dynamics. *Nat Rev Mol Cell Biol* 21: 204 – 224

Giroud M, Pisani DF, Karbiener M, Barquissau V, Ghandour RA, Tews D, Fischer-Posovszky P, Chambard JC, Knippschild U, Niemi T *et al* (2016) miR-125b affects mitochondrial biogenesis and impairs brite adipocyte formation and function. *Mol Metab* 5: 615 – 625

Giroud M, Tsokanos FF, Caratti G, Kotschi S, Khani S, Jouffe C, Vogl ES, Irmler M, Glantschnig C, Gil-Lozano M *et al* (2021) HAND2 is a novel obesity-linked adipogenic transcription factor regulated by glucocorticoid signalling. *Diabetologia* 64: 1850 – 1865

Giroud M, Jodeleit H, Prentice KJ, Bartelt A (2022) Adipocyte function and the development of cardiometabolic disease. *J Physiol* 600: 1189 – 1208

Higareda-Almaraz JC, Karbiener M, Giroud M, Pauler FM, Gerhalter T, Herzig S, Scheideler M (2018) Norepinephrine triggers an immediate-early regulatory network response in primary human white adipocytes. *BMC Genomics* 19: 794

Jespersen NZ, Larsen TJ, Peijs L, Daugaard S, Homoe P, Loft A, de Jong J, Mathur N, Cannon B, Nedergaard J *et al* (2013) A classical brown adipose tissue mRNA signature partly overlaps with brite in the supraclavicular region of adult humans. *Cell Metab* 17: 798 – 805

de Jong JMA, Sun W, Pires ND, Frontini A, Balaz M, Jespersen NZ, Feizi A, Petrovic K, Fischer AW, Bokhari MH *et al* (2019) Human brown adipose tissue is phenocopied by classical brown adipose tissue in physiologically humanized mice. *Nat Metab* 1: 830 – 843

Kazimierczyk M, Kasprowicz MK, Kasprzyk ME, Wrzesinski J (2020) Human long noncoding RNA interactome: detection, characterization and function. *Int J Mol Sci* 21: 1027

Keipert S, Kutschke M, Ost M, Schwarzmayr T, van Schothorst EM, Lamp D, Brachthauser L, Hamp I, Mazibuko SE, Hartwig S *et al* (2017) Long-term cold adaptation does not require FGF21 or UCP1. *Cell Metab* 26: 437 – 446.e5

Kirshner H, Aguet F, Sage D, Unser M (2013) 3-D PSF fitting for fluorescence microscopy: implementation and localization application. *J Microsc* 249: 13 – 25

Leitner BP, Huang S, Brychta RJ, Duckworth CJ, Baskin AS, McGehee S, Tal I, Dieckmann W, Gupta G, Kolodny GM *et al* (2017) Mapping of human brown adipose tissue in lean and obese young men. *Proc Natl Acad Sci USA* 114: 8649 – 8654

Liao Y, Smyth GK, Shi W (2014) featureCounts: an efficient general purpose program for assigning sequence reads to genomic features. *Bioinformatics* 30: 923 – 930

Liesa M, Shirihai OS (2013) Mitochondrial dynamics in the regulation of nutrient utilization and energy expenditure. *Cell Metab* 17: 491 – 506

Lo KA, Huang S, Walet ACE, Zhang ZC, Leow MK, Liu M, Sun L (2018) Adipocyte long-noncoding RNA transcriptome analysis of obese mice identified Lnc-leptin, which regulates leptin. *Diabetes* 67: 1045 – 1056

Love MI, Huber W, Anders S (2014) Moderated estimation of fold change and dispersion for RNA-seq data with DESeq2. *Genome Biol* 15: 550

MacDonald WA, Mann MRW (2020) Long noncoding RNA functionality in imprinted domain regulation. *PLoS Genet* 16: e1008930

Mahdaviani K, Benador IY, Su S, Gharakhanian RA, Stiles L, Trudeau KM, Cardamone M, Enriquez-Zarralanga V, Ritou E, Aprahamian T *et al* (2017) Mfn2 deletion in brown adipose tissue protects from insulin resistance and impairs thermogenesis. *EMBO Rep* 18: 1123 – 1138

van Marken Lichtenbelt WD, Vanhommerig JW, Smulders NM, Drossaerts JM, Kemerink GJ, Bouvy ND, Schrauwen P, Teule GJ (2009) Cold-activated brown adipose tissue in healthy men. *N Engl J Med* 360: 1500 – 1508

de Meis L (2001) Uncoupled ATPase activity and heat production by the sarcoplasmic reticulum Ca^{2+}-ATPase. Regulation by ADP. *J Biol Chem* 276: 25078 – 25087

Percie du Sert N, Hurst V, Ahluwalia A, Alam S, Avey MT, Baker M, Browne WJ, Clark A, Cuthill IC, Dirnagl U *et al* (2020) The ARRIVE guidelines 2.0: updated guidelines for reporting animal research. *BMJ Open Sci* 4: e100115

Pereira RO, Marti A, Olvera AC, Tadinada SM, Bjorkman SH, Weatherford ET, Morgan DA, Westphal M, Patel PH, Kirby AK *et al* (2021) OPA1 deletion in brown adipose tissue improves thermoregulation and systemic metabolism via FGF21. *Elife* 10: e66519

Petrovic N, Walden TB, Shabalina IG, Timmons JA, Cannon B, Nedergaard J (2010) Chronic peroxisome proliferator-activated receptor γ (PPARγ) activation of epididymally derived white adipocyte cultures reveals a population of thermogenically competent, UCP1-containing adipocytes molecularly distinct from classic brown adipocytes. *Journal of Biological Chemistry* 285: 7153 – 7164

Picelli S, Faridani OR, Bjorklund AK, Winberg G, Sagasser S, Sandberg R (2014) Full-length RNA-seq from single cells using Smart-seq2. *Nat Protoc* 9: 171 – 181

Pisani DF, Barquissau V, Chambard JC, Beuzelin D, Ghandour RA, Giroud M, Mairal A, Pagnotta S, Cinti S, Langin D *et al* (2018) Mitochondrial fission is

associated with UCP1 activity in human brite/beige adipocytes. *Mol Metab* 7: 35 – 44

Puigserver P, Wu Z, Park CW, Graves R, Wright M, Spiegelman BM (1998) A cold-inducible coactivator of nuclear receptors linked to adaptive thermogenesis. *Cell* 92: 829 – 839

Quiros PM, Ramsay AJ, Sala D, Fernandez-Vizarra E, Rodriguez F, Peinado JR, Fernandez-Garcia MS, Vega JA, Enriquez JA, Zorzano A *et al* (2012) Loss of mitochondrial protease OMA1 alters processing of the GTPase OPA1 and causes obesity and defective thermogenesis in mice. *EMBO J* 31: 2117 – 2133

Rocha N, Bulger DA, Frontini A, Titheradge H, Gribsholt SB, Knox R, Page M, Harris J, Payne F, Adams C *et al* (2017) Human biallelic MFN2 mutations induce mitochondrial dysfunction, upper body adipose hyperplasia, and suppression of leptin expression. *Elife* 6: e23813

Rogne M, Chu DT, Kuntziger TM, Mylonakou MN, Collas P, Tasken K (2018) OPA1-anchored PKA phosphorylates perilipin 1 on S522 and S497 in adipocytes differentiated from human adipose stem cells. *Mol Biol Cell* 29: 1487 – 1501

Ruan X, Li P, Chen Y, Shi Y, Pirooznia M, Seifuddin F, Suemizu H, Ohnishi Y, Yoneda N, Nishiwaki M *et al* (2020) In vivo functional analysis of non-conserved human lncRNAs associated with cardiometabolic traits. *Nat Commun* 11: 45

Sage D, Donati L, Soulez F, Fortun D, Schmit G, Seitz A, Guiet R, Vonesch C, Unser M (2017) DeconvolutionLab2: an open-source software for deconvolution microscopy. *Methods* 115: 28 – 41

Schmidt E, Dhaouadi I, Gaziano I, Oliverio M, Klemm P, Awazawa M, Mitterer G, Fernandez-Rebollo E, Pradas-Juni M, Wagner W *et al* (2018) LincRNA H19 protects from dietary obesity by constraining expression of monoallelic genes in brown fat. *Nat Commun* 9: 3622

Schmieder R, Edwards R (2011) Quality control and preprocessing of metagenomic datasets. *Bioinformatics* 27: 863 – 864

Seitz S, Kwon Y, Hartleben G, Julg J, Sekar R, Krahmer N, Najafi B, Loft A, Gancheva S, Stemmer K *et al* (2019) Hepatic Rab24 controls blood glucose homeostasis via improving mitochondrial plasticity. *Nat Metab* 1: 1009 – 1026

Shimizu I, Walsh K (2015) The whitening of brown fat and its implications for weight management in obesity. *Curr Obes Rep* 4: 224 – 229

Song Y, Milon B, Ott S, Zhao X, Sadzewicz L, Shetty A, Boger ET, Tallon LJ, Morell RJ, Mahurkar A *et al* (2018) A comparative analysis of library prep approaches for sequencing low input translatome samples. *BMC Genomics* 19: 696

Statello L, Guo CJ, Chen LL, Huarte M (2021) Gene regulation by long non-coding RNAs and its biological functions. *Nat Rev Mol Cell Biol* 22: 96 – 118

Sun L, Lin JD (2019) Function and mechanism of long noncoding RNAs in adipocyte biology. *Diabetes* 68: 887 – 896

Tajima K, Ikeda K, Tanabe Y, Thomson EA, Yoneshiro T, Oguri Y, Ferro MD, Poon ASY, Kajimura S (2020) Wireless optogenetics protects against obesity via stimulation of non-canonical fat thermogenesis. *Nat Commun* 11: 1730

Tang T, Yang L, Cao Y, Wang M, Zhang S, Gong Z, Xiong F, He Y, Zhou Y, Liao Q *et al* (2020) LncRNA AATBC regulates Pinin to promote metastasis in nasopharyngeal carcinoma. *Mol Oncol* 14: 2251 – 2270

Thaher O, Wolf C, Dey PN, Pouya A, Wullner V, Tenzer S, Methner A (2018) The thiol switch C684 in Mitofusin-2 mediates redox-induced alterations of mitochondrial shape and respiration. *Neurochem Int* 117: 167 – 173

Tran KV, Brown EL, DeSouza T, Jespersen NZ, Nandrup-Bus C, Yang Q, Yang Z, Desai A, Min SY, Rojas-Rodriguez R *et al* (2020) Human thermogenic adipocyte regulation by the long noncoding RNA LINC00473. *Nat Metab* 2: 397 – 412

U Din M, Saari T, Raiko J, Kudomi N, Maurer SF, Lahesmaa M, Fromme T, Amri EZ, Klingenspor M, Solin O *et al* (2018) Postprandial oxidative metabolism of human brown fat indicates thermogenesis. *Cell Metab* 28: 207 – 216.e3

Ukropec J, Anunciado RP, Ravussin Y, Hulver MW, Kozak LP (2006) UCP1-independent thermogenesis in white adipose tissue of cold-acclimated Ucp1−/− mice. *J Biol Chem* 281: 31894 – 31908

Virtanen KA, Lidell ME, Orava J, Heglind M, Westergren R, Niemi T, Taittonen M, Laine J, Savisto NJ, Enerback S *et al* (2009) Functional brown adipose tissue in healthy adults. *N Engl J Med* 360: 1518 – 1525

Wang M, Dai M, Wang D, Tang T, Xiong F, Xiang B, Zhou M, Li X, Li Y, Xiong W *et al* (2021) The long noncoding RNA AATBC promotes breast cancer migration and invasion by interacting with YBX1 and activating the YAP1/Hippo signaling pathway. *Cancer Lett* 512: 60 – 72

Weir G, Ramage LE, Akyol M, Rhodes JK, Kyle CJ, Fletcher AM, Craven TH, Wakelin SJ, Drake AJ, Gregoriades ML *et al* (2018) Substantial metabolic activity of human brown adipose tissue during warm conditions and cold-induced lipolysis of local triglycerides. *Cell Metab* 27: 1348 – 1355.e4

Wikstrom JD, Mahdaviani K, Liesa M, Sereda SB, Si Y, Las G, Twig G, Petrovic N, Zingaretti C, Graham A *et al* (2014) Hormone-induced mitochondrial fission is utilized by brown adipocytes as an amplification pathway for energy expenditure. *EMBO J* 33: 418 – 436

Yan K, Wang Y, Shao Y, Xiao T (2021) Gene instability-related lncRNA prognostic model of melanoma patients via machine learning strategy. *J Oncol* 2021: 5582920

Zhang B, Xu S, Liu J, Xie Y, Xiaobo S (2021) Long noncoding RNAs: novel important players in adipocyte lipid metabolism and derivative diseases. *Front Physiol* 12: 691824

Zhao F, Lin T, He W, Han J, Zhu D, Hu K, Li W, Zheng Z, Huang J, Xie W (2015) Knockdown of a novel lincRNA AATBC suppresses proliferation and induces apoptosis in bladder cancer. *Oncotarget* 6: 1064 – 1078

Zuriaga MA, Fuster JJ, Gokce N, Walsh K (2017) Humans and mice display opposing patterns of "browning" gene expression in visceral and subcutaneous white adipose tissue depots. *Front Cardiovasc Med* 4: 27